Comparative morphology of snake (Squamata) endocasts: evidence of phylogenetic and ecological signals

Rémi Allemand, Renaud Boistel, Gheylen Daghfous, Zoé Blanchet, Raphael Cornette, Nathalie Bardet, Peggy Vincent, Alexandra Houssaye

Comparative morphology of snake (Squamata) endocasts: evidence of phylogenetic and ecological signals

Rémi Allemand[1,2,*], Renaud Boistel[3], Gheylen Daghfous[4], Zoé Blanchet[2], Raphaël Cornette[5], Nathalie Bardet[1], Peggy Vincent[1], Alexandra Houssaye[2]

[1]Centre de Recherches sur la Paléobiodiversité et les Paléoenvironnements, CR2P - UMR 7207 - CNRS, MNHN, UPMC, Muséum National d'Histoire Naturelle, Sorbonne Universités, 57 rue Cuvier, CP38, F-75005, Paris, France

[2]UMR 7179 – CNRS / Muséum National d'Histoire Naturelle, Département Adaptations du Vivant, 57 rue Cuvier, CP55, F-75005, Paris, France

[3]IPHEP-UMR CNRS 6046, UFR SFA, Université de Poitiers, 40 avenue du Recteur Pineau, F-86022, Poitiers, France

[4]Groupe de Recherche sur le Système Nerveux Central, Département de Neurosciences, Université de Montréal, Montréal, Québec, Canada

[5]Institut de Systématique, Evolution, Biodiversité, ISYEB – UMR 7205 – CNRS, MNHN, UPMC, EPHE, Muséum National d'Histoire Naturelle, Sorbonne Universités, 57 rue Cuvier, CP50, F-75005, Paris, France

** Corresponding author: remi.allemand@edu.mnhn.fr*

Abstract

Brain endocasts obtained from computed tomography are now widely used in the field of comparative neuroanatomy. They provide an overview of the morphology of the brain and associated tissues located in the cranial cavity. Through anatomical comparisons between species, insights on the senses, the behavior, and the lifestyle can be gained. Although there are many studies dealing with mammal and bird endocasts, those performed on the brain endocasts of squamates are comparatively rare, thus limiting our understanding of their morphological variability and interpretations. Here, we provide the first comparative study of snake brain endocasts in order to bring new information about the morphology of these structures. Additionally, we test if the snake brain endocast encompasses a phylogenetic and/or an ecological signal. For this purpose, the digital endocasts of 45 snake specimens, including a wide diversity in terms of phylogeny and ecology, were digitized using computed tomography, and compared both qualitatively and quantitatively. Snake endocasts exhibit a great variability. The different methods performed from descriptive characters, linear measurements and the outline curves provided complementary information. All these methods have shown that the shape of the snake brain endocast contains, as in mammals and birds, a phylogenetic signal but also an ecological one. Although phylogenetically-related taxa share several similarities between each other, the brain endocast morphology reflects some notable ecological trends: e.g., 1) fossorial species possess both reduced optic tectum and pituitary gland; 2) both fossorial and marine species have cerebral hemispheres poorly developed laterally; 3) cerebral hemispheres and optic tectum are more developed in arboreal and terrestrial species.

Key words: computed tomography, brain endocast, snakes, morphometrics, ecological signal, squamates, sensory information.

Introduction

Computed Tomography (CT) allows the reconstruction of high-quality 3D models of both hard and soft tissues that can be used for different purposes, such as anatomical and biomechanical studies. It thus constitutes an important exploratory tool in biology and opens a range of new possible investigations (e.g., Boistel et al., 2011a; Carril et al., 2015).

Computed tomography is now widely used to visualize the endocranial space with the construction of digital endocasts that may reflect the morphology of the brain and associated tissues (e.g., Anderson et al., 2000; Macrini et al., 2007; Olori, 2010; Bienvenu et al., 2011; Smith & Clarke, 2012; Racicot & Colbert, 2013; Ahrens, 2014; Carril et al., 2015; Corfield et al., 2015; Danilo et al., 2015; Gonzales et al., 2015, Kawabe et al., 2015), the inner ear (e.g., Chapla et al., 2007; Georgi & Sipla, 2008; Walsh et al., 2009; Ekdale, 2010, 2011, 2013; Willis et al., 2013), the vascular system (e.g., Porter & Witmer, 2015), the cranial nerves (e.g., George & Holliday, 2013), and pneumatic sinuses (e.g., Bona et al., 2013). Endocasts are generated at the interface between the skeleton (typically bone or cartilage) and the soft tissues (or fluid) lying immediately near it (Balanoff et al., 2015). In the cranial cavity, the soft tissue forming the interface with the surrounding skeleton is not the brain but the superficial surface of the dural meninges, blood vessels and vasculature enveloping the brain (Walsh & Knoll, 2011). Thus, brain endocasts provide only an overview of the external morphology of the brain itself. They may reflect the relative size of the different regions of the brain and could provide some information about sensory abilities, as well as about the behavior and ecology of the species (Walsh & Knoll, 2011).

The degree to which the brain endocast reflects the morphology of the brain depends on the degree to which the brain fills the cranial cavity. This factor can vary widely between lineages (e.g., Jerison, 1973; Hopson, 1979; Witmer et al., 2008; George & Holliday, 2013) and over ontogeny (e.g., Macrini et al., 2007; Hurlburt et al., 2013). From different age

classes, the brain of the marsupial *Monodelphis domestica* fills between 67.8 and 86.6% of the endocranial volume (Macrini et al., 2007), whereas that of the smallest alligators occupies about 68% of the endocranial space, and about 32% in the largest alligators (Hurlburt et al., 2013). Mammals and birds, which are generally considered as highly encephalized taxa (large brains relative to body size, Balanoff et al., 2015), tend to have brains that nearly fill the cranial cavity, resulting in a strong correlation between the volume and morphology of the brain endocast and those of the brain (Balanoff et al., 2015). Thus, similarly as the brain morphology that may reflect the influence of ecological, behavioral and/or phylogenetic factors (e.g. Lefebvre et al., 2004; Walsh & Milner, 2011), the brain endocast of these taxa tends to have both a phylogenetic and ecologic signals (Lyras & Van Der Geer, 2003; Macrini et al., 2007; Carril et al., 2015; Corfield et al., 2015). Additionally, there is an increasing number of studies performed from brain endocasts of mammals and birds. These studies are generally performed to understand the relation between the mass of the brain and the volume of the cast, but also to consider the intraspecific variability, reflecting either ontogenetic variation, sexual dimorphism, or both (e.g., Macrini et al. 2007; Bienvenu et al., 2011; Kawabe et al., 2015), or finally focusing on the interspecific variability (e.g., Kawabe et al., 2013).

Among vertebrates other than mammals and birds, it is generally admitted that the brain does not entirely fill the cranial cavity (Balanoff et al., 2015). A commonly cited estimate considers that the brain occupies only 50% of the endocranial space (Hopson, 1979). However, this ratio is only based on the observation of one *Sphenodon* and one *Iguana* brain specimens (Hurlburt et al., 2013), and is probably far from representing a general pattern in non-endotherms. For example, it has been shown that the brain almost entirely fills the endocranial space in some extant chondrichthyans and teleosts (Northcutt, 2002; Balanoff et al., 2015). Within Squamata (lizards, snakes and amphisbaenians), a wide range of brain

versus endocranial cavity proportions were found (Kim & Evans, 2014). The lowest brain–endocranial volume ratio is found in *Gecko gecko* (0.35), whereas the false monitor lizard *Callopistes maculatus* exhibits a brain that nearly fills the endocranial cavity (0.97). Moreover, snakes and amphisbaenians are known to have a brain that fills most of the endocranial space (Starck, 1979; Nieuwenhuys et al., 1998), with a very narrow space between the brain and the cranial wall. The brain may thus fill the intracranial cavity in some squamates, indicating that brain endocasts within these species may reflect the external morphology of the brain with a certain degree of accuracy.

Computed tomography (i.e., magnetic resonance imaging (MRI) and X-ray absorption, as well as X-ray phase-contrast imaging techniques) has already been used on skulls of squamates for different purposes, such as the study of the brain (e.g., Anderson et al., 2000), the ear (e.g., Walsh et al., 2009; Boistel et al., 2011b; Christensen et al., 2012; Yi & Norell, 2015), and the skull morphology (e.g., Rowe et al., 1999; Bever et al., 2005; Rieppel & Maisano, 2007; Comeaux et al., 2010), the vascular patterns (e.g., Porter and Witmer, 2015), and the lacrimal system (e.g., Souza et al., 2015). But to date only a single study has focused on the brain endocast (Olori, 2010). In her study, Olori reconstructed and described the endocast of the burrowing snake *Uropeltis woodmasoni* and thus provided the first description of a snake brain endocast. However, as no comparative data are available within squamates, the results obtained cannot be discussed in detail. To date, there are several studies published about the brain itself or the central nervous system of squamates (e.g., Senn, 1966; Senn & Northcutt, 1973; Hoogland, 1982; Smeets et al., 1986; Martinez-Garcia et al., 1991; Reperant et al., 1992; Lanuza & Halpern, 1997; Nieuwenhuys et al., 1998; Atobe et al., 2004; Butler & Hodos, 2005; Powell & Leal, 2014) but the exact relationship between brain endocasts and brain morphology remains currently untested for squamates. In addition, data about the brain endocast morphology in this clade are insufficient to fully interpret this structure.

The present contribution proposes the first brain endocast comparative study in squamates. It will focus on snakes that are of particular interest since they show a great diversity in morphology, and occupy a wide range of ecologies with e.g., fossorial, aquatic, and arboreal species (e.g., Heatwole, 1999; Greene et al., 2000). Here, we propose to provide a quantitative anatomical description of the brain endocast of a wide sample of snake species using different morphometric approaches in order to: 1) bring new information about this structure, its general traits within snakes and the variation occurring; 2) test if, as in mammals and birds, the brain endocast of snakes reflects a phylogenetic and/or ecologic signal.

Material and Methods

Material

The material consists of the skull of 45 snake specimens (38 genera and 43 species; see Table 1); illustrating the diversity of snakes in both phylogenetic and ecological (i.e., habitat) perspectives (see Fig. 1). The dataset is divided into six fossorial, seven arboreal, thirteen terrestrial, nine semi-aquatic and ten marine species (Heatwole, 1999; Houssaye et al., 2013; Anthony Herrel, pers. com.). The semi-aquatic group encompasses species that spend most of their time in freshwater without contact with the sea. Three specimens of a single species, *Python regius*, were analyzed in order to evaluate the intraspecific variation.

Data acquisition

Microtomography was performed in order to non-destructively digitize the brain endocast of the specimens. The skull of the specimens studied were scanned: (1) at the University of Poitiers (France), Institut de Chimie des Milieux et Matériaux of Poitiers (IC2MP, Poitiers, France) using a X8050-16 Viscom model (resolution between 16.7 and 32.3 µm; reconstructions performed using Feldkamp algorithm with DigiCT software, version 1.15

[Digisens SA, France]); and (2) at the European Synchrotron Radiation Facility (ESRF, Grenoble, France) using third generation synchrotron microtomography on beamlines ID 19 and BM5 (resolution between 5.0 and 14.9 μm; reconstructions performed using filtered back-projection algorithm with the ESRF PyHST software).

Image segmentation and visualization were performed using VGStudioMax 2.2 (Volume Graphics Inc., Heidelberg, Germany) at the Palaeontology Imaging Unit of the MNHN/UMR 7207 CR2P and Avizo 7.0 (VSG, Burlington MA, USA) at the UMR 7179 MECADEV. The segmentation tools of these software packages were used to select the endocranial space of the specimens thereby allowing separation of the skull from the endocranial space, and to reconstruct the brain endocast.

Institutional abbreviations

IC2MP, Institut de Chimie des Milieux et Matériaux, Poitiers, France; **ESRF**, European Synchrotron Radiation Facility, Grenoble, France ; **MCZ**, Museum for Comparative Zoology, Harvard University, U. S. A.; **MNHN**, Muséum National d'Histoire Naturelle, Paris, France ; **ZRC**, Zoological Reference Collections, National University of Singapore.

Measurements

For each specimen, 21 measurements were defined and taken to illustrate the whole 3D shape, volume and surface of the brain endocast (see Fig. 2B). All the measurements made on the brain endocast were measured point-to-point and obtained with the digital caliper of VGStudioMax 2.2 and the measuring tool of Avizo 7.0, both with accuracy of 0.01mm (see Supporting information S1 & S2). The print of the sutures between the different skull bones visible on the brain endocast surface were used to define homologous distances. The following list introduces the measurements taken on the brain endocast. The different parts of

176 the brain endocast are named with the same terms as those used for the brain itself (see Fig.
177 2A), following Butler & Hodos (2005); however the terms used here do not have a
178 neurological significance and are not related to neural structures.
179 (a) *Length of the brain endocast* **(LE)**: distance between the anteriormost part of the
180 olfactory bulbs still entirely surrounded by the frontal bone and the tip of the suture left by the
181 contact of the supraoccipital with the two exoccipitals on the dorsal surface of the brain
182 endocast;
183 (b) *Length of the olfactory bulbs* **(LOB)**: distance between the anteriormost part of the
184 olfactory peduncles still entirely surrounded by the frontal bone and the fronto-parietal suture;
185 (c) *Length of the groove between the olfactory bulbs* **(LG)**: distance between the
186 anteriormost end of the groove between the olfactory peduncles and the fronto-parietal suture;
187 (d) *Height of the main olfactory bulb* **(HOB)**: at the level of the anteriormost part of
188 the main olfactory bulb still entirely surrounded by the frontal bone;
189 (e) *Height of the olfactory peduncle* **(HOP)**: at the level of the fronto-parietal suture;
190 (f) *Width of the olfactory peduncles* **(WOP)**: at the level of the fronto-parietal suture;
191 (g) *Length of the fissura interhemispherica* **(LFI)**: distance between the fronto-parietal
192 suture and the virtual limit made by the groove between the cerebral hemispheres and the
193 optic tectum;
194 (h) *Maximal width of the cerebral hemispheres* **(WCH)**;
195 (i) *Lateral expansion of the cerebral hemispheres* **(LCH)**: distance between the
196 fronto-parietal suture and the posterior end of the lateral margin of the cerebral hemispheres;
197 (j) *Maximal height of the cerebral hemispheres* **(HCH)**;
198 (k) *Maximal width of the optic tectum* **(WOR)**;

(l) *Length of the optic tectum* **(LOR)**: distance between the virtual limit made by the groove separating the cerebral hemispheres of the optic tectum (see Fig. 2B) and the tip of the V-shaped suture between the parietal and the supraoccipital (see Fig. 2A);

(m) *Height of the optic tectum* **(HOR)**: distance between the dorsal surface of the optic tectum and the triple point formed by the suture between the parietal, prootic and basisphenoid (see Fig. 2A);

(n) *Length of the pituitary gland* **(LP)**: distance between the fronto-parietal suture and the most posterior point of the pituitary bulb;

(o) *Height of the pituitary gland* **(HP)**: distance between the most ventral point of the pituitary gland and the triple point formed by the sutures between the parietal, prootic and basisphenoid;

(p) *Width of the inner ear region* **(WIE)**: distance between the two triple points formed by the sutures of the supraoccipital, prootic and exoocipital;

(q) *Dorsal width of the posterior end of the brain endocast* **(DWPE)**: distance taken at the level of the suture between the supraoccipital and the two exoccipitals seen on the dorsal surface of the brain endocast;

(r) *Length of the posterior part of the brain endocast* **(LPE)**: distance between the tip of the V-shaped suture between the parietal and the supraoccipital, and the tip of the V-shaped suture between the supraoccipital and the two exoccipitals;

(s) *Height of the posterior part of the brain endocast* **(HPE)**: distance between the maximum of concavity of the inner ear region and the ventral margin of the brain endocast;

(t) *Width of the ventral part of the brain endocast* **(WPE)**: distance between the two triple points formed by the suture between the prootic, basisphenoid and basioccipital on the ventral margin;

(u) *Width in the pituitary gland region* **(WP)**: distance taken on the ventral surface of the brain endocast, between the triple points formed by the sutures between the parietal, prootic and basisphenoid.

Quantitative analyses

In order to provide complementary information, three different approaches were used to study the brain endocast variability occurring in snakes.

Descriptive character analysis

The differences observed between the various snake brain endocasts were listed and coded (See Supporting information S3: List of the characters and Matrix). We used the coded characters to run a principal coordinate analysis (PCoA) in order to evaluate the distances between the taxa and thus to identify which taxa are similar in brain endocast morphology based on these coded characters: the closest the species, the more similar the brain endocast morphologies.

Measure analysis

All data (see Supporting information S1 & S2) were log10-transformed prior to analysis to meet assumptions of normality and homoscedasticity required for parametric analyses. All the analyses were performed using the statistic software R (R Development Core Team, 2008). To analyze shape components independently from size, the log-shape ratios (Mosimann & James, 1979) were calculated based of the raw log10-transformed linear dimensions of the brain endocast.

In order to take into account the biases induced by measurement repeatability, three specimens of *Python regius* showing the lowest shape variation were selected. According to

248 the data published by Aubret et al. (2005), the comparison of their jaw length seems to
249 differentiate a neonate specimen (P1; jaw length = 25.4 mm) from a juvenile (P3; jaw length
250 = 31.4 mm) and an adult (P2; jaw length = 40.3 mm) ones. Ten repetitions were performed for
251 each measure on these three specimens. Then, to quantify and visualize the differences
252 between repetitions, a Principal Component Analysis (PCA) was performed. Shape
253 differences between specimens were much higher than shape differences induced by
254 repetitions (see Supporting information S2).
255 To evaluate the phylogenetic signal in the shape on the brain endocast in snakes, we
256 used a multivariate generalization of the K statistic of Blomberg et al. (2003): the *K*mult
257 (Adams, 2014). The phylogenetic signal is based on a phylogenetic consensus tree derived
258 from several published phylogenies (Pyron et al., 2011; Hsiang et al., 2015; Lee & Scanlon,
259 2002; Fig. 1). Adams (2014) demonstrated that values of *K*mult <1 imply that taxa resemble
260 each other phenotypically less than expected under Brownian motion whereas values of
261 *K*mult >1 imply that close relatives are more similar to one another phenotypically than
262 expected under Brownian motion. A PCA was also performed on the data obtained from the
263 measurements made on the 45 snake specimens; the mean of the 10 measurements taken on
264 each of the *Python regius* specimens was used.
265 To test the relationships between the habitat/ecology and the morphology of the brain
266 endocast, the sampled taxa were classified into five habitat categories (see Fig.1): fossorial,
267 terrestrial, arboreal, semi-aquatic, and marine (Heatwole, 1999; Houssaye et al., 2013; A.
268 Herrel, pers. comm.). We performed a standard and phylogenetic MANOVA, to respectively
269 evaluate whether the brain endocast variability could reflect the ecology, taking or not the
270 phylogenetic relationships into consideration.
271
272 *Outline curve analysis*

For each brain endocast, the ventral and lateral views were selected to perform an outline curve analysis using geometric morphometrics (Zelditch et al., 2004). We used 2D sliding semi-landmarks (Gunz & Mitteroecker, 2013) that permit accurate description of homologous anatomical curves devoid of anatomical landmarks. Sliding semi-landmarks are allowed to slide, minimizing the bending energy between each specimen and the mean shape of the data set. This step creates a geometric homology between specimens that permits all classical geometric morphometric analyses. We performed a General Procrustes Superimposition to work on shape (Rohlf, & Slice, 1990) and PCAs for each view.

The dorsal view was not used here because of the difficulty to distinguish homologous outline curves on the posterior part of the structure at the level of the inner ear position. In ventral view, the 45 brain endocasts of our dataset were used. In lateral view, we used the posterior crest formed by the inner ear and three homologous points as landmarks to facilitate the placement of the curve semilandmarks. The sutures between the different skull bones visible on the posterior part of the brain endocast surface were used to define homologous points. The first point corresponds to the triple point formed by the sutures between the basioccipital, exoccipital and prootic. The second is the triple point formed by the prootic, the basioccipital and the basisphenoid. The last point represents the most ventral point of the suture between the basioccipital and the basisphenoid. In lateral view, we used 38 specimens because the sutures are not visible and did not allow the placement of the same landmarks on *Aipysurus eidouxii*, *Cerebrus rynchops*, *Corallus hortulanus*, *Dispholidus typus*, *Mimophis mahfalensis*, the smallest specimen of *Python regius* and *Uropeltis pulneyensis*.

Results

General description of snake endocast and variability

Here, only a description of the brain endocast will be provided, without considering the cranial nerves or the inner ear (data in Boistel et al., 2011b; Yi & Norell, 2015). The cast of the endocranial space does not only reflect the brain itself: associated tissues (e.g., venous system) are also reconstructed during segmentation and may hide some parts of the brain. The endocast morphology resulting from the segmentation of the endocranial space is described below as a whole. The brain endocast in snakes is surrounded dorsally by the frontal and parietal (anteriorly) and the supraoccipital and exoccipital (posteriorly), laterally by the prootics, and ventrally by the basioccipital and para-basisphenoid. The surface of the brain endocast of snakes is smooth.

Telencephalon

The telencephalon includes the olfactory bulbs, the olfactory peduncles and the cerebral hemispheres (see Fig. 2A). The main and accessory olfactory bulbs correspond to the anteriormost structure of the brain endocast (see Fig. 2A); however, from the brain endocast only it is not possible to distinguish one from another. They are attached to the rostral pole of the cerebral hemisphere by short olfactory peduncles. In dorsal view, a groove is visible running between the two olfactory bulbs. Posteriorly, the cerebral hemispheres represent the largest part of the brain endocast and gradually widen laterally. An interhemispheric fissure may be visible on the dorsal surface of the brain endocast, as attested by a groove between the cerebral hemispheres. The length of the interhemispheric fissure and the depth of the groove vary according to taxa.

Some taxa may exhibit olfactory bulbs wider than long, giving a short and stout aspect (e.g., width/length aspect ratio superior to one in *Typhlophys squamosus*, see Fig. 4A) in

dorsal view, while most taxa have an olfactory structure longer than wide (e.g., width/length aspect ratio inferior to one in *Hierophis viridiflavus*, see Fig. 4B). The lateral margin of this structure may be mediolaterally convex (e.g., *Acrochordus granulatus*, see Fig. 4D), relatively straight (e.g., *Eunectes murinus*, see Fig. 4E) or mediolaterally concave (e.g., *Hierophis viridiflavus*, see Fig. 4B) in dorsal view. Most species possess in dorsal view a system composed of two parallel olfactory bulbs and peduncles (e.g., *Eunectes murinus*, see Fig. 4E). Some others show a projection that diverges laterally from the fronto-parietal suture (e.g., *Homalopsis buccata*, see Fig. 4F), whereas others share the two conditions with parallel olfactory bulbs and peduncles diverging laterally at their anterior end (e.g., *Hierophis viridiflavus*, see Fig. 4B). In lateral view, the ventral margin may be ventrodorsally concave (e.g. *Mimophis mahfalensis*, see Fig. 5D), convex (e.g., *Boiga dendrophila*, see Fig. 5B) forming a bulge, or straight (e.g., *Homalopsis buccata*, see Fig. 5C). Some taxa (e.g., *Typhlophys squamosus*, see Fig. 4A) do not show any separation over the whole length of the olfactory peduncles in dorsal view. Most taxa have olfactory peduncles diverging only at their anterior end (e.g., *Hierophis viridiflavus*, see Fig. 4B). Some species have a large space between the two olfactory structures, separating them along almost their entire length (e.g., *Acrochordus granulatus*, see Fig. 4D). The width of the olfactory bulbs may vary antero-posteriorly. At the level of the fronto-parietal suture and in dorsal view, some taxa possess a posterior part as wide (e.g., *Eunectes murinus*, see Fig. 4E) or wider (e.g., *Cylindrophis ruffus*, see Fig. 4C) than the anterior end. However, others have olfactory bulbs with an anterior end wider than the posterior part (e.g., *Hierophis viridiflavus*, see Fig. 4B).

The relative size of the cerebral hemispheres varies between taxa. A distinction is seen between those that have hemispheres wider than long (e.g., width/length aspect ratio close to 1.4 in *Chrysopelea ornata*, see Fig. 4G) and those that have a structure as long as wide (e.g., width/length aspect ratio close to one in*Typhlophys squamosus*, see Fig. 4A). A

few taxa are exceptions with cerebral hemispheres longer than wide (e.g., width/length aspect ratio close to 0.3 in *Cylindrophis ruffus*, see Fig. 4C). The lateral extension in dorsal view generally begins just posterior to the fronto-parietal suture (e.g., *Eunectes murinus*, see Fig. 4E) but two taxa (*Cylindrophis ruffus* [Fig. 4C] and *Anilius scytale* [Fig. 4H]) exhibit cerebral hemispheres with an anterior part as wide as the fronto-parietal suture, the lateral extension occurring more posteriorly. In dorsal view, the lateral margin may be rounded (e.g., *Eunectes murinus*, see Fig. 4E) or relatively straight (e.g., *Chrysopelea ornata*, see Fig. 4G), providing a square appearance to the cerebral hemispheres. In lateral view, differences occur between taxa with cerebral hemispheres developed only along the horizontal axis (e.g., *Typhlophys squamosus*, see Fig. 5A), taxa with cerebral hemispheres developed in the horizontal plane but with a posterior part directed ventrally (e.g., *Homalopsis buccata*, see Fig. 5C) and taxa with a dorso-ventral extension at least as long as the horizontal one (e.g., *Boiga dendrophila*, see Fig. 5B). The limit between the cerebral hemispheres and the optic tectum depends on the lateral extension of the cerebral hemispheres. Species that do not have an important lateral extension (e.g., *Anilius scytale*, see Fig. 4H) do not show a clear delimitation between the optic tectum and the cerebrum, contrary to those that have a groove between the two structures and have laterally extended cerebral hemispheres (e.g., *Chrysopelea ornata*, see Fig. 4G).

Diencephalon

The pituitary gland, located ventrally to the cerebral hemispheres, is the only structure of the diencephalon seen on the brain endocast (see Fig. 2A); the pineal gland is not visible. In addition, the external morphology of the brain endocast does not allow the hypothalamus and the hypophysis to be delimited.

The pituitary gland may be marked by the presence in lateral view of a small bulge on the ventral surface of the brain endocast (e.g., *Anilius scytale*, see Fig. 5E). But generally the system shows a structure more developed ventrally, displaying (e.g., *Hierophis viridiflavus*, see Fig. 5F) or not (e.g., *Eunectes murinus*, see Fig. 5G) a posterior projection. Among those displaying a posterior projection, a distinction is made between those presenting a tilted system (e.g., *Enhydrina schistosa*, see Fig. 5H) and those having a posterior projection in the horizontal plane (e.g., *Hierophis viridiflavus*, see Fig. 5F). Differences relative to the ventral margin of the posterior projection also occur, between a curved (e.g., *Thamnophis sirtalis*, see Fig. 5J) and a flat (e.g., *Dispholidus typus*, see Fig. 5I) shape.

Mesencephalon

The mesencephalon lies posterior to the cerebral hemispheres. The optic tectum forms the roof of the mesencephalon (see Fig. 2A). From the endocast, the distinction between the optic tectum and the tegmentum, which is located more ventrally in the mesencephalon, is not possible. In dorsal view, the mesencephalon is less wide than the cerebral hemispheres.

In a few taxa this structure is not distinguishable from the cerebral hemispheres (e.g., *Typhlophys squamosus*, see Fig. 4A). In some others, the structure is visible in dorsal view only thanks to its decrease in width as compared to the cerebral hemispheres (e.g., *Eunectes murinus*, see Fig. 4E), and its surface appears smooth and flattened. However, in other species, the optic tectum exhibits in dorsal view a pair of domes separated by a median sulcus (e.g., *Thamnophis sirtalis*, see Fig. 6A). Some taxa show (in dorsal view) a distinct optic tectum as wide as the rhombencephalon (e.g. *Homalopsis buccata*, see Fig. 4F). The others have an optic tectum wider (e.g., *Chrysopelea ornata*, see Fig. 4G) or narrower (e.g., *Acrochordus granulatus*, see Fig. 4D) than the ventral margin of the rhombencephalon. In lateral view, most taxa possess a dorsal margin of the optic tectum located at the same height

394 as the cerebral hemispheres (e.g., *Eunectes murinus*, see Fig. 5G), except *Erpeton*
395 *tentaculatum*, in which the margin is located more dorsally (see Fig. 6D).
396
397 *Rhombencephalon*
398 Posterior to the optic tectum, the cerebellum is not visible on the dorsal surface of the
399 brain endocast. According to Aurboonyawat et al. (2008), the dorsal longitudinal vein located
400 on the mid-dorsal surface of the brain endocast must cover it. On the lateral sides of the brain
401 endocast, the large and round impressions indicate the position of the inner ear (see Fig. 2A).
402 The *medulla oblongata* is located ventral to the inner ear region, and represents the ventral
403 margin of the posterior part of the brain endocast.
404 Most species exhibit a rhombencephalon in lateral view with a rounded (e.g., *Boa*
405 *constrictor*, see Fig. 7A) or straight (e.g., *Erpeton tentaculatum*, see Fig. 6D) ventral margin,
406 but in some taxa (e.g., *Crotalus atrox*, see Fig. 7B) the ventral margin is triangular, pointing
407 ventrally. The ventral extension of the *rhombencephalon* may correspond to the most ventral
408 surface of the brain endocast in lateral view (e.g., *Boa constrictor*, see Fig. 7A) or not (e.g.,
409 *Dispholidus typus*, see Fig. 5I).
410
411 **Quantitative analyses**
412 Brain endocasts of snakes show a great variability. This variability is characterized by
413 different relative proportions between the structures visible on the brain endocasts (e.g., size
414 of the optic tectum compared to that of the cerebral hemispheres), giving a wide range of
415 shapes, from stout (e.g., *Typhlophis squamosus*), to elongated and gracile (e.g., *Pelamis*
416 *platurus*) or elongated and wide (e.g., *Boa constrictor*) brain endocasts. Below, this variability
417 is analyzed quantitatively.

418

419 *Descriptive character analysis*

420 The results obtained (Fig. 8) show that 50.3 % of the variance is explained by the two
421 main principal components (29.4 % and 20.9 % respectively). The distribution of the taxa
422 indicates that fossorial and marine snakes are both distinct from those with other ecologies.
423 Among the fossorial species, *Atractaspis irregularis* is quite distinct from two groups: the
424 first one including *Uropeltis pulneyensis*, *Cylindrophis ruffus*, and *Anilius scytale*, and the
425 second one made by *Typhlophis squamosus* and *Rhinotyphlops schlegelii*. *Micrurus*
426 *lemniscatus* and *Acrochordus granulatus*, a terrestrial and a semi-aquatic snakes, respectively,
427 tend toward the brain endocast morphology found in the fossorial taxa. Among the marine
428 species of our dataset, *Enhydrina schistosa* and *Microcephalophis gracilis* are close to each
429 other and distinct from other marine snakes. The terrestrial species show a wide distribution.
430 The isolated position of *M. lemniscatus* was already cited above. *Hierophis gemonensis*,
431 *Hierophis viridiflavus*, and *Thamnophis sirtalis* are close together and located near the two
432 arboreal snakes *Dispholidus typus* and *Chrysopelea ornata*. These species are distinct from
433 *Mimophis mahfalensis*, *Crotalus atrox*, *Agkistrodon contortrix*, *Coronella austriaca* and *Naja*
434 *nivea*, which are close together and possess a brain endocast morphology similar to the
435 arboreal snakes *Boiga dendrophila* and *Dasypeltis* sp. In addition, the three specimens of
436 *Python regius* and *Candoia* sp., are distinct from the other terrestrial taxa with a brain
437 endocast morphology tending towards those found in marine ones. Among the arboreal taxa
438 not cited above, *Corallus hortulanus*, *Boa constrictor* and *Pareas margaritophorus* are close
439 to the semi-aquatic snake *Cantoria violacea*. The distribution of the semi-aquatic species
440 overlaps those of the terrestrial and arboreal snakes. The brain endocast of *Enhydris enhydris*
441 is similar to that of *M. mahfalensis* and distinct from those of *Erpeton tentaculum*, *Fordonia*
442 *leucobalia*, *Homalopsis buccata*, and *Enhydris punctata*, which are grouped together. The two

443 species *Cerberus rynchops* and *Eunectes murinus* are respectively close to *Candoia* sp. and to
444 the three specimens of *P. regius*, and tend towards the marine taxa.
445 The species distribution suggests the existence of phylogenetic and ecological signals.
446 Phylogenetically close species show more similarities than with other species (e.g.,
447 *Typhlophis squamosus* and *Rhinotyphlops schlegelii*). However, an ecological signal is also
448 perceived, meaning that species sharing the same ecology show more brain endocast
449 similarities than species with a different ecology.
450
451 *Measure analysis*
452 Intraspecific variability in *Python regius*
453 The PCA (see Fig. 9) shows that the two main axes explain 93 % of the variance (80
454 % and 13 % respectively). The repeatability test is positive as the ten iterations for each
455 specimen are clearly grouped and the three specimens clearly distinct, indicating that the
456 variability caused by the measurement acquisition is inferior to the variability between the
457 specimens. All variables seem to act on the distribution of the specimens (though the impact
458 of LP (Length of the pituitary bulb) on the second axis appears significantly more important
459 than that of the other variables). The first principal component mostly separates the specimens
460 based on size. The variables principally acting on PCA1 are the height of the olfactory bulbs
461 (HOB), the length of the optic tectum (LOR) and the length of the pituitary gland (LP). The
462 smaller specimen (P1) has the greatest height of the olfactory bulbs, the greatest length of the
463 pituitary bulb, and the smallest length of the optic tectum. The second principal component
464 separates the intermediate specimen (P3) from the two others. The main variable acting along
465 the second axis is still the length of the pituitary gland (LP). The intermediate specimen (P3)
466 shows the smallest height of the olfactory bulb, the greatest length of the optic tectum and an
467 intermediate value for the length of the pituitary gland. Finally, the largest specimen (P2)

possesses the greatest length of the pituitary gland, and intermediate values for the height of the olfactory bulb and for the length of the optic tectum.

Interspecific variability

The PCA obtained with all snake specimens (see Fig. 10) shows that 60 % of the variance is explained by the two first axes (44.7% and 15.3% respectively). Fossorial species are clearly distinct from the others, with a great distribution along the first axis, contrary to the snakes with other ecologies, that all display a more limited distribution. The PCA shows some overlap between the snakes with arboreal, terrestrial, semi-aquatic and marine habitats, but a gradation is clearly visible. The arboreal and terrestrial taxa appear distinct (with no overlap) from the marine ones. All variables seem to act on the repartition of the species (see Supporting information S4). However, along the first axis, two variables mostly act on the distribution of the taxa: the width at the optic tectum level (WOR) and the dorsal width of the posterior end of the brain endocast (DWPE). The first axis seems to separate species that have an optic tectum as wide as the posterior end of the brain endocast (e.g., *Typhlophis squamosus*) from the ones in which the optic tectum is much wider than the posterior end of the brain endocast (e.g., *Pelamis platurus*). Along the second axis, the width of the olfactory peduncles (WOP) and the width of the cerebral hemispheres (WCH) explain most of the variability. These variables allow to distinguish species presenting a large difference between the width of the olfactory peduncles and the width of the cerebral hemispheres (e.g., *Boa constrictor*), from those that have a smaller difference between these two widths (e.g., *Cylindrophis ruffus*).

The MANOVA performed on the data indicates significant differences between brain endocasts depending on ecology (MANOVA: Wilks $\lambda = 0.751$, $F_{2, 22} = 8.75$, $P = 0.013$). The Kmult test indicates that brain endocast shape in snakes exhibits a significant phylogenetic

493 signal (Kmult = 0.814; P.value = 0.001), showing the importance to consider the phylogeny in
494 studies of snake brain endocasts. The phylogenetic MANOVA still indicates significant
495 differences pending on ecology (phylogenetic MANOVA: Wilks $\lambda = 0.0074$, $F_{2, 22} = 81.748$,
496 Pphyl = 0.0087).
497
498 *Outline curve analysis*
499 The results obtained by the outline curve analyses (Fig. 11 and 12) enable to comment
500 on the shape of snake brain endocasts according to the different ecologies.
501 The first PCA is obtained from the endocast outline curves in ventral view (Fig. 11)
502 and shows that 61.9% of total variance is explained by the two first axes (44.6% and 17.3%
503 respectively). The first axis separates proportionally stout brain endocasts, wide at the level of
504 the olfactory bulbs and of the cerebral hemispheres (blue dotted line, Fig. 11, Axis 1), from
505 longer and narrower endocasts (black dotted line, Fig. 11, Axis 1). Thus, brain endocasts of
506 semi-aquatic, arboreal and terrestrial snakes are mostly wide, whereas the fossorial and
507 marine species have an extended distribution along this first axis, encompassing both wide
508 and narrow endocasts. However, the distribution of marine taxa is mainly concentrated
509 towards narrow endocasts and only two species, *Aipysurus duboisii* and *Aipysurus eydouxii*,
510 move towards wide endocasts. Along the second axis, the shape of the forebrain (olfactory
511 bulbs and cerebral hemispheres) principally drives the distribution. Brain endocasts with wide
512 olfactory bulbs have cerebral hemispheres located more anteriorly (dark dotted line, Fig. 11,
513 Axis 2) than those with thinner olfactory bulbs (blue dotted line, Fig. 11, Axis 2). Semi-
514 aquatic, fossorial and marine species all exhibit a brain endocast with wide olfactory bulbs
515 and anteriorly located cerebral hemispheres, contrary to the arboreal and terrestrial snakes that
516 are distributed all along the axis and thus express the two conditions.

The second PCA is obtained from the endocast outline curves in lateral view (Fig. 12) and shows that 65.8% of total variance is explained by the two first axes (48% and 17.8% respectively). The first axis illustrates brain endocasts with well dorsoventrally developed and ventrally oriented olfactory bulbs, and a posterior part characterized by a rounded dorsal surface more developed dorsally than the anterior part (blue dotted line in Fig. 12, Axis 1). These brain endocasts differ from those in which the olfactory bulbs are less developed dorsoventrally and dorsally oriented, and the posterior part presents a flat dorsal surface located at the same level as the anterior part (dark dotted line Fig. 12, Axis 1). The brain endocast of the fossorial species *Rhinotyphlops schlegelii* is well distinct from those of other taxa, with a structure very developed dorsoventrally and the posterior region higher than the anterior one. Arboreal and terrestrial species may show a mix between the two morphologies, with a well dorsoventrally developed brain endocast but a flat posterior region located at the same level as the anterior one. Marine snakes tend to have a flat brain endocast, whereas semi-aquatic and fossorial taxa show a large distribution presenting the two brain endocast morphologies. The second axis separates stout brain endocasts well developed dorsoventrally, with a slight dorsal constriction at the limit between the olfactory bulbs and the cerebral hemispheres (blue dotted line Fig. 12, Axis 2) from longer but less dorsoventrally developed brain endocasts (dark dotted line Fig. 12, Axis 2), with a ventral constriction at the limit between the olfactory bulbs and the cerebral hemispheres. The distribution of the taxa seems to indicate that the two morphologies are variably found in all ecologies. However, the dorsoventrally compressed brain endocast found in both marine (*Pelamis platurus*) and terrestrial (*Candoia* sp.) snakes, differs from the more dorsoventrally developed brain endocasts found in other taxa sharing their ecologies.

Discussion

Phylogenetic signal

We detected a significant phylogenetic signal in the snake brain endocast variability, meaning that it is at least partly constrained by shared ancestry. Indeed, some patterns or main trends in the brain endocast morphology reflect snakes' systematics. The scolecophidian snakes (*R. schlegelii* and *T. squamosus*, see Fig. 1) are the only ones presenting a brain endocast where the optic tectum is not visible (see Fig. 4A). Within the Booidae (see Fig. 1), the surface of the optic roof is smooth (e.g., *Eunectes murinus*, see Fig. 4E), and the pituitary gland is only developed ventrally. The Hydrophiidae (see Fig. 1) have cerebral hemispheres poorly developed laterally (e.g., *Enhydrina schistosa*, see Fig. 5H), contrary to the Colubridae (see Fig. 1) that possess cerebral hemispheres very developed both laterally and ventrally (e.g., *Hierophis viridiflavus*, see Fig. 4B, 5F), as well as an optic roof clearly visible with two distinct domes, and the olfactory bulbs widening on their anterior part. As the multivariate K was lower than one, species resemble each other less than expected under a Brownian motion model of evolution, which shows that, though significant, the phylogenetic signal remains weak. This suggests that other factors, such as ecology, do affect the snake endocast morphology.

Ecological signal

We also detected an ecological signal in the brain endocast of snakes, even when the phylogenetic relationships were taken into account. Though the different ecologies tested here are thus associated with morphological trends of the brain endocast, it nevertheless appears difficult to associate one structure with one ecology. Both standard and phylogenetic MANOVAs indicate significant differences between the ecologies, with an impact of all variables on the distribution of snakes. Thus, fossorial species have a brain endocast with a

poor lateral development of the cerebral hemispheres, and not visible or absent optic tectum and pituitary gland. Marine species exhibit an endocast more elongated, with cerebral hemispheres poorly developed laterally and projected only in the antero-posterior plan, but the optic tectum is clearly visible and the pituitary gland is developed ventrally. Brain endocasts of terrestrial and arboreal snakes differ from marine ones' by the great lateral extension of the cerebral hemispheres. Finally, it appears difficult to distinguish a common pattern for semi-aquatic snakes.

Within the same ecology, a great variability in brain endocast morphology can be observed. The results obtained from the outline curve analysis (Fig. 11 and 12) provide some examples. The cerebral hemispheres of *Aipysurus duboisii* and *Aipysurus eydouxii* are wider than long and developed ventrally on their posterior part, whereas in the other marine taxa of our dataset, the cerebral hemispheres are as long as wide and only directed in the horizontal plane. The brain endocasts of *Pelamis platurus* and *Candoia* sp. appear more flattened than those respectively found in other marine and terrestrial species. Finally, the morphology, the proportions and the orientation of the brain endocast of *Rhinotyphlops schlegelii* appear very distinct from those found in other fossorial snakes. It appears difficult to interpret these differences. It has been demonstrated that constraints imposed by the environment (e.g., habitat) and activity pattern have an impact in snake head shape, irrespective of the phylogenetic relationships (Fabre et al., 2016; Segall et al., 2016). These ecological constraints affect the brain endocast morphology in snakes as well. However, it is difficult to determine with certainty which ecological parameters mostly affect the brain endocast morphology. The two marine species, *A. duboisii* and *A. eydouxii,* have a brain endocast quite different from other marine taxa. It is unclear if these differences are related to changes in their skull morphology due to the fish-egg dietary specialization (Sanders et al., 2012) or if the particular morphology of their cerebral hemispheres has a sensory meaning. Similarly, the

591 flattened brain endocast of *Pelamis platurus*, not found in any other marine specimen from
592 our dataset, could be related to modifications in the skull morphology associated with its
593 pelagic condition, only known in this species, or to its unique foraging strategy at the oceanic
594 surface through labile features such as slicks or drift lines (Brischoux & Lillywhite, 2011). It
595 will be interesting to decompose the ecology in different factors (e.g., locomotion, prey
596 capture mode) to determine which parameters mostly influence the snake brain endocast
597 morphology.
598
599 **Sensory inferences**
600 Studies in mammals and birds have shown that the endocast morphology, like the
601 brain morphology, may give some information about species sensory abilities (Sakai et al.,
602 2011a,b; Corfield et al., 2012, 2015; Carril et al., 2015). Several studies on snake brain have
603 shown a link between structure and function (e.g., Kubie et al., 1978; Halpern & Frumin,
604 1979; Halpern & Kubie, 1979; Friedman & Crews, 1985; Krohmer & Crews, 1987; Crews et
605 al., 1988; Miller & Gutzke, 1999; Wyneken, 2007; Krohmer et al., 2010) but the link between
606 sensory abilities and brain endocasts has never been investigated in snakes. According to
607 Starck (1979) and Nieuwenhuys et al. (1998), the brain of snakes could fill the majority of the
608 endocranial space, and thus reflect the brain anatomy. If it is the case, brain endocasts could
609 provide information about their sensory abilities. The relationships between the brain and the
610 brain endocast is currently untested in snakes (Olori, 2010), and was not the goal of this study.
611 In snakes, the main olfactory bulb (MOB) is responsible for capturing smells at the
612 level of the olfactory epithelium, and transmitting them to the olfactory bulb; the accessory
613 olfactory bulb (AOB) is responsible for pheromone processing related to chemical social
614 communication and prey capture (Bales, 2014). The MOB projects mainly to the lateral cortex
615 and the AOB mainly to the *nucleus sphericus* (Lanuza & Halpern, 1997), two structures

616 localized in the cerebral hemispheres. The MOB and AOB are involved in different
617 behavioral activities, such as predation, mating and courtship (Bales, 2014). It is difficult to
618 clearly identify the two structures and their limits from the brain endocast. However,
619 morphological differences are perceived between the sampled taxa and they may imply
620 differences in their sensory abilities. All snakes have a very developed vomeronasal system
621 (Kubie & Halpern, 1979; Bales, 2014); however in hydrophiinae sea snakes the main
622 olfactory bulbs are considered to be functionless and it seems that they use the AOB for
623 smelling underwater (Schwenk, 2008; Schichida et al., 2013). Brain endocasts of
624 hydrophiidae are indeed the only ones to show olfactory bulbs with a width increasing along
625 the antero-posterior axis (e.g., *Enhydrina schistosa*, see Fig. 5H), which could correspond to a
626 reduced MOB and a more developed AOB.
627 The cerebral hemispheres of snakes are composed of different structures (e.g., cortex,
628 nucleus sphericus, anterior ventricular ridge, amygdala), each being considered as a link
629 between the sources of sensory information and the brain structures that control and modulate
630 the behavior (Halpern, 1980; Bales, 2014). Different studies about the lizard brain have
631 shown that the medial dorsal cortices are relatively bigger in active foragers (Day et al.,
632 1999a,b; 2001; Ladage et al., 2009). In snakes, males, which have a larger average territory
633 than females, possess a significantly larger medial cortex than females (Roth et al., 2006).
634 However, all these internal structures are not distinguishable on endocasts. Moreover, no
635 comparative studies on snake brain endocasts have been performed to correlate size variation
636 of these inner neural structures with endocast morphology. It is thus difficult to evaluate
637 whether the different morphologies exhibited by the cerebral hemispheres of snakes involve
638 differences in their sensory abilities.
639 The optic tectum in snakes is involved in the production of natural orienting
640 movements in response to somatosensory, visual, and auditory stimuli (Nieuwenhuys et al.,

1998; Wyneken, 2007), and to signals from the infrared sensory system found in some snake families (Boidae, Pythonidae, and Crotalinae) (Goris, 2011). Several authors have shown that the size of the optic tectum is correlated to some behavioral traits and ecologies (Masai, 1973; Nieuwenhuys et al., 1998). For instance diurnal species have a larger optic tectum than burrowing species. From snake endocasts, it actually appears that all fossorial species have a reduced optic tectum, (e.g., *Cylidrophis ruffus*, see Fig. 4C), contrary to terrestrial and arboreal taxa, which have a large optic tectum (e.g., *Chrysopelea ornata*, see Fig. 4G). According to Lillywhite (2014), vision is better developed in arboreal snakes, and poorly developed in burrowing species and some aquatic species living in turbid waters. It seems thus possible to connect the size of the optic tectum to the development of vision. According to Masai (1973), the optic tectum of diurnal snakes is, as a rule, larger than that of nocturnal ones. However, the correlation between large optic tectum and diurnal activity is not clear. Some exceptions exist: the endocast of *Boiga dendrophila* (see Fig. 5B), a nocturnal snake (Rodda et al., 1999; Shivik et al., 2000), also shows a large optic tectum. There seems also to be no correlation between the occurrence of an infrared sensory system and the size of the optic tectum on endocasts. Specimens that have infrared organs (e.g., *Crotalus atrox*, see Fig. 7B) do not exhibit a larger optic tectum than specimens without infrared organs (e.g., *Boa constrictor*, see Fig. 7A). There is however one exception: *Erpeton tentaculatum* (see Fig. 6B-D), the only specimen which has an endocast with the dorsal margin of the optic tectum located more dorsally than the dorsal margin of the cerebral hemispheres. Such features can be correlated to the special nature of *E. tentaculatum*, which is the only snake presenting a pair of appendages that protrude from the face (Catania, 2011; 2012). The tentacles, useful to detect and locate preys, are innervated by trigeminal fibers to the optic tectum and could be responsible for its large size in *E. tentaculatum*.

Snake endocasts also show a great variability in the pituitary gland. This structure is generally considered to be structurally and functionally the most complex organ of the endocrine system (Harris & Donovan, 1966). Among vertebrates, the pituitary of snakes possesses some unique features: an asymmetrical structure flattened dorsoventrally and a pars tuberalis never developed (Schreibman, 1986). From the observation of brain endocasts only, a large variability is observed. However, it is not possible to determine whether this variability has a sensory significance. For example, brain endocasts of fossorial specimens have a clearly reduced pituitary gland but it is not clear whether this morphology is an adaptation reflecting the specialization of the skull due to fossorial activity (Rieppel, 1979; Rieppel & Zaher, 2000) or if this morphology has a sensory implication.

It is tempting to interpret the brain endocast variability in snakes through differences in sensory abilities between species; however, it is necessary to be very careful in the sensory inferences brought by an endocast study, which gives only an overview of the external morphology of the brain, and the complexity of the structure(s) must be taken into account.

Perspectives

The rapidly expanding interest in, and availability of, digital tomography data to visualize casts of the vertebrate endocranial cavity housing the brain (endocasts) represent new opportunities and challenges to the field of comparative neuroanatomy (Balanoff et al., 2015). In snakes, the brain endocast is still poorly known and the information associated with this structure remains untested. The different approaches used here have shown that snake brain endocasts contain both phylogenetic and ecological signals. However, the degree of influence of these two signals on the brain endocast morphology is difficult to interpret. It will be interesting to dissociate the variability due to each signal. Moreover, to fully understand the brain endocast structure and its variability among snakes, it appears necessary to

decompose the ecology in different parameters (e.g., locomotion, prey capture mode) in order to test whether one is particularly associated to one brain endocast structure.

Beyond the methodological approaches that we used in this study, the resort to three-dimensional geometric morphometrics (3DGM) would be interesting to improve the amount of shape changes taken into consideration. However, the difficulty of finding homologous anatomical landmarks would impose the use of sliding semi landmarks on surfaces (Gunz & Mitteroecker, 2013).

Cranial endocasts also represent a potentially large amount of unexplored phylogenetic data. Most morphological data for phylogenetic analyses of vertebrates come from the exterior shape of the skull (e.g., Gauthier et al., 2012). Internal cranial morphology is poorly represented in phylogenetic analyses because of the difficulty in visualizing and studying this anatomy. The advent of CT technology provides the potential to incorporate these new data into phylogenetic analyses.

Finally, in the context of the strong debate about the phylogenetic and ecological origin of snakes (e.g., Lee et al., 1999; Conrad, 2008; Hsiang et al., 2015; Martill et al., 2015; Reeder et al., 2015; Yi and Norell, 2015), endocranial studies might be of strong interest. Their application on crown snakes and lineages closely related to snakes (i.e., varanids, dibamids, mosasauroids) would provide major complementary information.

Conclusion

We used different methods to describe the brain endocast of snakes: descriptive characters, outline curve analysis, measurement series, and we observed a great variability in the brain endocast morphology of snakes. These methods provided different complementary information but all have shown that the shape of this structure contains, as in mammals and birds, a phylogenetic signal but also an ecological one. The different trends observed in the

brain endocast morphology distinguish the different ecologies, notably fossorial and marine snakes. The great diversity observed in the brain endocast of snakes, even within the same ecology, appears difficult to interpret and further analyses on the relation between brain endocast and ecological and sensory factors will be required. Biological inferences based on this structure should thus be made with caution and it is important to understand the complexity of this structure in order to avoid quick potentially wrong assumptions.

Acknowledgements

This work was supported by a grant from Agence Nationale de la Recherche under the LabEx ANR-10-LABX-0003-BCDiv, in the program "Investissements d'avenir" n° ANR-11-IDEX-0004-02. We thank I. Ineich (MNHN, Paris, France), J. Rosado (MCZ, Harvard, U. S. A), K. Lim (ZRC, National University of Singapore) and A. Herrel (MNHN, Paris, France) for the loan of specimens and already digitized snake data. We thank the Steinmann-Institut (Universität Bonn, Bonn, Germany), the UMS 2700 outils et méthodes de la systématique intégrative CNRS-MNHN and AST-RX, Plateau technique d'accès scientifique à la tomographie à rayons X du MNHN, and the ESRF (Grenoble, France; beamline ID17) and Paul Tafforeau for providing beamtime and support. We are also thankful to the 3D platform (UMR 7207, CR2P, MNHN) for giving access to the 3D imaging facilities. Finally, we want to thank both reviewers for helpful comments and suggestions.

Author contributions

Research conception and design: A. H., N. B., P. V.

Data acquisition: A. H., R. A., R. B., G. D.

Data analysis and interpretation: A. H., R. A., R.C., Z. B.

Drafting of the manuscript: R. A.

Critical revision of the manuscript: All authors.

Conflict of interest

The authors declare no conflict of interest.

References

Adams DC (2014) A generalized K statistic for estimating phylogenetic signal from shape and other high-dimensional multivariate data. *Systematic Biology* **63**, 685–697.

Ahrens HE (2014) Morphometric study of phylogenetic and ecologic signals in Procyonid (Mammalia: Carnivora) endocasts: morphometrics of Procyonid endocasts. *The Anatomical Record* **297**, 2318–2330.

Anderson CL, Kabalka GW, Layne DG, Dyke JP, Burghardt GM (2000) Noninvasive high field MRI brain imaging of the Garter Snake (*Thamnophis sirtalis*). *Copeia*, **2000**, 265–269.

Atobe Y, Nakano M, Kadota T et al. (2004) Medullary efferent and afferent neurons of the facial nerve of the Pit Viper *Gloydius brevicaudus*. *The journal of Comparative Neurology* **472**, 345–357.

Aubret F, Bonnet X, Harris M, Maumelat S (2005) Sex differences in body size and ectoparasite load in the ball python, *Python regius*. *Journal of Herpetology* **39**, 315–320.

Aurboonyawat T, Pereira V, Kring T et al. (2008) Patterns of the Cranial Venous System from the Comparative Anatomy in Vertebrates: Part II. The Lateral-Ventral Venous System. *Interventional Neuroradiology*, **14**, 21–31.

Balanoff AM, Bever GS, Colbert MW et al. (2015) Best practices for digitally constructing endocranial casts: examples from birds and their dinosaurian relatives. *Journal of Anatomy* **229**, 173–190.

764 **Bales TB** (2014) Proliferation, migration and survival of cells in the telencephalon of the ball
765 python, *Python regius*. *PhD Thesis*, 131pp.
766 **Bever GS, Bell CJ, Maisano JA** (2005) The ossified braincase and cephalic osteoderms of
767 *Shinisaurus crocodilurus* (Squamata, Shinisauridae). *Palaeontologia Electronica* **8**, 1–36.
768 **Bienvenu T, Guy F, Coudyzer W et al.** (2011) Assessing endocranial variations in great apes and
769 humans using 3D data from virtual endocasts. *American Journal of Physical Anthropology*
770 **145**, 231–246.
771 **Blomberg SP, Garland T, Ives AR** (2003) Testing for phylogenetic signal in comparative data:
772 behavioral traits are more labile. *Evolution* **57**, 717–745.
773 **Boistel R, Swoger J, Krzic U et al.** (2011a) The future of three-dimensional microscopic imaging
774 in marine biology. *Marine Ecology* **32**, 438–452.
775 **Boistel R, Herrel A, Lebrun R et al.** (2011b) Shake rattle and roll: the bony labyrinth and aerial
776 descent in Squamates. *Integrative and Comparative Biology* **51**, 957–968.
777 **Bona P, Degrange FJ, Fernández MS** (2013) Skull anatomy of the bizarre Crocodylian
778 *Mourasuchus nativus* (Alligatoridae, Caimaninae): skull anatomy of *Mourasuchus nativus*.
779 *The Anatomical Record* **296**, 227–239.
780 **Brischoux F, Lillywhite HB** (2011) Light- and flotsam-dependent 'float-and-wait' foraging by
781 pelagic sea snakes (Pelamis platurus). *Marine Biology* **158**, 2343–2347.
782 **Butler AB, Hodos W** (2005) Comparative Vertebrate Neuroanatomy: Evolution and Adaptation.
783 *John Wiley & Sons, Inc., Hoboken, NJ, USA*, 744 pp.
784 **Carril J, Tambussi CP, Degrange FJ, Benitez Saldivar MJ, Picasso MBJ** (2015) Comparative
785 brain morphology of Neotropical parrots (Aves, Psittaciformes) inferred from virtual 3D
786 endocasts. *Journal of Anatomy* **229**, 1–13.
787 **Catania KC** (2011) The brain and behavior of the tentacled snake. *Annals of the New York*
788 *Academy of Sciences* **1225**, 83–89.

Catania KC (2012) Tactile sensing in specialized predators – from behavior to the brain. *Current Opinion in Neurobiology* **22**, 251–258.

Chapla ME, Nowacek DP, Rommel SA, Sadler VM (2007) CT scans and 3D reconstructions of Florida manatee (*Trichechus manatus latirostris*) heads and ear bones. *Hearing Research* **228**, 123–135.

Christensen CB, Christensen-Dalsgaard J, Brandt C, Teglberg Madsen P (2012) Hearing with an atympanic ear: good vibration and poor sound-pressure detection in the royal python, *Python regius*. *The Journal of Experimental Biology* **215**, 331–342.

Comeaux RS, Olori JC, Bell CJ (2010) Cranial osteology and preliminary phylogenetic assessment of *Plectrurus aureus* Beddome, 1880 (Squamata: Serpentes: Uropeltidae). *Zoological Journal of the Linnean Society* **160**, 118–138.

Conrad JL (2008) Phylogeny and systematics of Squamata (Reptilia) based on morphology. *Bulletin of the American Museum of Natural History* **310**, 1–182.

Corfield JR, Wild JM, Parsons S, Kubke MF (2012) Morphometric analysis of telencephalic structure in a variety of Neognath and Paleognath bird species reveals regional differences associated with specific behavioral traits. *Brain, Behavior and Evolution* **80**, 181–195.

Corfield JR, Price K, Iwaniuk A et al. (2015) Diversity in olfactory bulb size in birds reflects allometry, ecology and phylogeny. *Frontiers in Neuroanatomy* **9**, doi:10.3389/fnana.2015.00102.

Crews D, Hingorani V, Nelson RJ (1988) Role of the pineal gland in the control of annual reproductive behavioral and physiological cycles in the Red-Sided Garter Snake (*Thamnophis sirtalis parietalis*). *Journal of Biological Rhythms* **3**, 293–302.

Danilo L, Remy J, Vianey-Liaud M, Mérigeaud S, Lihoreau F (2015) Intraspecific variation of endocranial structures in extant Equus: A prelude to endocranial studies in fossil Equoids. *Journal of Mammalian Evolution* **22**, 561–582.

Day LB, Crews D, Wilczynski W (1999a) Relative medial and dorsal cortex volume in relation to foraging strategy in congeneric lizards. *Brain, Behavior and Evolution* **54**, 314–322.

Day LB, Crews D, Wilczynski W (1999b) Spatial and reversal learning in congeneric lizards with different foraging strategies. *Animal Behaviour* **57**, 395–407.

Day LB, Crews D, Wilczynski W (2001) Effects of medial and dorsal cortex lesions on spatial memory in lizards. *Behavioural Brain Research* **118**, 27–42.

Ekdale EG (2010) Ontogenetic variation in the bony labyrinth of *Monodelphis domestica* (Mammalia: Marsupialia) following ossification of the inner ear cavities. *The Anatomical Record: Advances in Integrative Anatomy and Evolutionary Biology* **293**, 1896–1912.

Ekdale EG (2011) Morphological variation in the ear region of pleistocene elephantimorpha (Mammalia, Proboscidea) from central Texas. *Journal of Morphology* **272**, 452–464.

Ekdale EG (2013) Comparative anatomy of the bony labyrinth (inner ear) of placental mammals. *PLoS One* **8**, e66624.

Fabre A-C, Bickford D, Segall M, Herrel A (2016) The impact of diet, habitat use, and behaviour on head shape evolution in homalopsid snakes. *Biological Journal of the Linnean Society* **118**, 634–647.

Friedman D, Crews D (1985) Role of the anterior hypothalamus–preoptic area in the regulation of courtship behavior in the male Canadian red-sided garter snake (*Thamnophis sirtalis parietalis*): Lesion experiments. *Behavioral neuroscience* **99**, 942–949.

Gauthier JA, Kearney M, Maisano JA, Rieppel O, Behlke ADB (2012) Assembling the squamate tree of life: Perspectives from the phenotype and the fossil record. *Bulletin of the Peabody Museum of Natural History* **53**, 3–308.

George ID, Holliday CM (2013) Trigeminal nerve morphology in *Alligator mississippiensis* and its significance for Crocodyliform facial sensation and evolution. *The Anatomical Record* **296**, 670–680.

Georgi JA, Sipla J (2008) Comparative and functional anatomy of balance in aquatic reptiles and birds. In *Sensory Evolution on the Threshold: Adaptations in Secondarily Aquatic Vertebrates,* Thewissen JMG, Numella S. Berkeley: University of California Press. pp. 233–256.

Gonzales LA, Benefit BR, McCrossin ML, Spoor F (2015) Cerebral complexity preceded enlarged brain size and reduced olfactory bulbs in Old World monkeys. *Nature Communications* **6**, 1-9.

Goris RC (2011) Infrared organs of snakes: An integral part of vision. *Journal of Herpetology* **45**, 2–14.

Greene HW, Fogden M, Fogden P (2000) Snakes: The Evolution of Mystery in Nature. *University of California Press*, 365pp.

Gunz P, Mitteroecker P (2013) Semilandmarks: a method for quantifying curves and surfaces. *Hystrix, the Italian Journal of Mammalogy* **24**, 103–109.

Halpern M (1980) The telencephalon of snakes. In S. O. E. Ebbesson (ed) Comparative Neurology of the telencephalon. Springer US, 257–295.

Halpern M, Frumin N (1979) Roles of the vomeronasal and olfactory system in prey attack and feeding garter snakes. *Physiology & Behavior* **22**, 1183–1189.

Halpern M, Kubie JL (1980) Chemical access to the vomeronasal organs of Garter snakes. *Physiology & Behavior* **24**, 367–371.

Harris GW, Donovan BT (1966) The pituitary gland: anterior pituitary. *University of California Press*, 444–459.

Heatwole H (1999) Sea snakes. *Krieger Publishing Company*, 148pp.

Hoogland PV (1982) Brainstem afferents to the thalamus in a lizard, *Varanus exanthematicus*. *The journal of Comparative Neurology* **210**, 152–162.

Hopson JA (1979) Paleoneurology. In C. Gans, R.G. Northcutt and P. Ulinski (eds) *Biology of the Reptilia (Neurology A)*. Academic Press, New York 9, 39–146.

Houssaye A, Boistel R, Böhme W, Herrel A (2013) Jack-of-all-trades master of all? Snake vertebrae have a generalist inner organization. *Naturwissenschaften* **100**, 997–1006.

Hsiang AY, Field DJ, Webster TH et al. (2015) The origin of snakes: revealing the ecology, behavior, and evolutionary history of early snakes using genomics, phenomics, and the fossil record. *BMC Evolutionary Biology* **15**, 1–22.

Hurlburt GR, Ridgely RC, Witmer LM (2013) Relative size of brain and cerebrum in tyrannosaurid dinosaurs: an analysis using brain-endocast quantitative relationships in extant alligators. In Parrish JM, Molnar RE, Currie PJ, Koppelhus EB (eds) *Tyrannosaurid Paleobiology*, Bloomington: Indiana University Press, 1–21.

Jerison H (1973) Evolution of the brain and intelligence. Academic Press, New York, 482 pp.

Kawabe S, Shimokawa T, Miki H, Matsuda S, Endo H (2013) Variation in avian brain shape: relationship with size and orbital shape. *Journal of Anatomy* **223**, 495–508.

Kawabe S, Matsuda S, Tsunekawa N, Endo H (2015) Ontogenetic shape change in the chicken brain: Implications for paleontology. *PLOS ONE* **10**, e0129939.

Kim R, Evans D (2014) Relationships among brain, endocranial cavity, and body sizes in reptiles. *Society of Vertebrate Paleontology 74th Annual Meeting*, Berlin, Germany.

Krohmer RW, Crews D (1987) Temperature activation of courtship behavior in the male red-sided garter snake (*Thamnophis sirtalis parietalis*): Role of the anterior hypothalamus-preoptic area. *Behavioral neuroscience* **101**, 228–236.

Krohmer RW, Boyle MH, Lutterschmidt DI, Mason RT (2010) Seasonal aromatase activity in the brain of the male red-sided garter snake. *Hormones and Behavior* **58**, 485–492.

Kubie JL, Vagvolgyi A, Halpern M (1978) Roles of the vomeronasal and olfactory systems in courtship behavior of male garter snakes. *Journal of Comparative and Physiological Psychology* **92**, 627–641.

Kubie JL, Halpern M (1979) Chemical senses involved in Garter snake prey trailing. *Journal of Comparative and Physiological Psychology* **93**, 648–667.

Ladage LD, Riggs BJ, Sinervo B, Pravosudov VV (2009) Dorsal cortex volume in male side-blotched lizards (*Uta stansburiana*) is associated with different space use strategies. *Animal behaviour* **78**, 91–96.

Lanuza E, Halpern M (1997) Afferent and efferent connections of the nucleus sphericus in the snake *Thamnophis sirtalis*: Convergence of olfactory and vomeronasal information in the lateral cortex and the amygdala. *The journal of Comparative Neurology* **385**, 627–640.

Lee MS, Scanlon JD (2002) Snake phylogeny based on osteology, soft anatomy and ecology. *Biological Review* **77**, 333–401.

Lee MS, Bell Jr. GL, Caldwell MW (1999) The origin of snake feeding. *Nature* **400**, 655–659.

Lefebvre L, Reader SM, Sol D (2004) Brains, innovations and evolution in birds and primates. *Brain, Behavior and Evolution* **63**, 233–246.

Lillywhite HB (2014) How snakes work: structure, function, and behavior of the world's snakes. *Oxford University Press*, 256pp.

Lyras GA, Van Der Geer AAE (2003) External brain anatomy in relation to the phylogeny of Caninae (Carnivora: Canidae). *Zoological Journal of the Linnean Society* **138**, 505–522.

Macrini TE, Rowe T, VandeBerg JL (2007) Cranial endocasts from a growth series of *Monodelphis domestica* (Didelphidae, Marsupialia): A study of individual and ontogenetic variation. *Journal of Morphology* **268**, 844–865.

Martill DM, Tischlinger H, Longrich NR (2015) A four-legged snake from the Early Cretaceous of Gondwana. *Science* **349**, 416–419.

Martinez-Garcia F, Olucha FE, Teruel V, Lorente MJ, Schwerdtfeger WK (1991) Afferent and efferent connections of the olfactory bulbs in the lizard *Podarcis hispanica*. *The journal of Comparative Neurology* **305**, 337–347.

Masai H (1973) Structural patterns of the optic tectum in Japanese snakes of the family Colubridae in relation to habit. *Journal Für Hirnforschung* **14**, 367–374.

Miller LR, Gutzke WHN (1999) The role of the vomeronasal organ of crotalines (Reptilia: Serpentes: Viperidae) in predator detection. *Animal Behaviour* **58**, 53–57.

Mosimann JE, James FC (1979) New Statistical Methods for Allometry with Application to Florida Red-Winged Blackbirds. *Evolution* **33**, 444–459.

Nieuwenhuys R, ten Donkelaar HJ, Nicholson C (1998) *The Central Nervous System of Vertebrates*. Berlin: Springer, 2214pp.

Northcutt RG (2002) Understanding Vertebrate Brain Evolution. *Integrative and Comparative Biology* **42**, 743–756.

Olori JC (2010) Digital Endocasts of the Cranial Cavity and Osseous Labyrinth of the Burrowing Snake *Uropeltis woodmasoni* (Alethinophidia: Uropeltidae). *Copeia* **2010**, 14–26.

Porter WR, Witmer LM (2015) Vascular Patterns in Iguanas and Other Squamates: Blood Vessels and Sites of Thermal Exchange. *PLOS ONE* **10**, e0139215.

Powell BJ, Leal M (2014) Brain Organization and Habitat Complexity in Anolis Lizards. *Brain Behavior and Evolution* **84**, 8–18.

Pyron RA, Burbrink FT, Colli GR et al. (2011) The phylogeny of advanced snakes (Colubroidea), with discovery of a new subfamily and comparison of support methods for likelihood trees. *Molecular Phylogenetics and Evolution* **58**, 329–342.

R Development Core Team (2008) R: A language and environment for statistical computing. R Foundation for Statistical Computing, Vienna, Austria. ISBN 3-900051-07-0, http://www.R-project.org.

Racicot RA, Colbert MW (2013) Morphology and Variation in Porpoise (Cetacea: Phocoenidae) Cranial Endocasts. *The Anatomical Record* **296**, 979–992.

Reeder TW, Townsend TM, Mulcahy DG et al. (2015) Integrated analyses resolve conflicts over squamate reptile phylogeny and reveal unexpected placements for fossil taxa. *PLOS ONE* **10**, e0118199.

Reperant J, Rio J-P, Ward R et al. (1992) Comparative Analysis of the Primary Visual System of Reptiles. In C. Gans and P. S. Ulinski (eds) *Sensory Integration. Biology of Reptilia, (Neurology C)*. The University of Chicago Press **7**, 175–240.

Rieppel O (1979) The braincase of Typhlops and Leptotyphlops (Reptilia: Serpentes). *Zoological Journal of the Linnean Society* **65**, 161–176.

Rieppel O, Zaher H (2000) The braincases of mosasaurs and Varanus, and the relationships of snakes. *Zoological Journal of the Linnean Society* **129**, 489–514.

Rieppel O, Maisano JA (2007) The skull of the rare Malaysian snake Anomochilus leonardi Smith, based on high-resolution X-ray computed tomography. *Zoological Journal of the Linnean Society* **149**, 671–685.

Rodda GH, Fritts TH, McCoid MJ, Campbell III EW (1999) An Overview of the Biology of the Brown Treesnake (*Boiga irregularis*), a Costly Introduced Pest on Pacific Islands. In Rodda, G. H., Sawai, Y.; Chiszar, D. & Tanaka, H. (eds) Problem snake management: the habu and the brown treesnake. Cornell University Press, Ithaca, NY, 534pp.

Rohlf FJ, Slice D (1990) Extensions of the Procrustes method for the optimal superimposition of landmarks. *Systematic Biology* **39**, 40–59.

Roth ED, Lutterschmidt WI, Wilson DA (2006) Relative Medial and Dorsal Cortex Volume in Relation to Sex Differences in Spatial Ecology of a Snake Population. *Brain Behavior and Evolution* **67**, 103–110.

Rowe T, Brochu CA, Colbert M et al. (1999) Introduction to Alligator: Digital atlas of the skull. Journal of Vertebrate Paleontology **19**, 1–8.

Sakai ST, Arsznov BM, Lundrigan BL, Holekamp KE (2011a) Brain Size and Social Complexity: A Computed Tomography Study in Hyaenidae. *Brain, Behavior and Evolution* **77**, 91–104.

Sakai ST, Arsznov BM, Lundrigan BL, Holekamp KE (2011b) Virtual endocasts: an application of computed tomography in the study of brain variation among hyenas: Hyena endocasts. *Annals of the New York Academy of Sciences* **1225**, 160–170.

Sanders KL, Rasmussen AR, Elmberg J et al. (2012) *Aipysurus mosaicus*, a new species of egg-eating sea snake (Elapidae: Hydrophiinae), with a redescription of *Aipysurus eydouxii* (Gray, 1849). *Zootaxa* **3431**, 1–18.

Schreibman MP (1986) The Pituitary Gland. In: Pang PKT, Schreibman MP (eds) Vertebrate Endocrinology: Fundamentals and Biomedical Implications, Vol. I. Academic Press, New York, 11–55.

Schwenk K (2008) Comparative anatomy and physiology of chemical senses in nonavian aquatic reptiles. In Thewissen, J.G.M., Nummela, S. (eds.) Sensory Evolution on the Threshold: Adaptations in Secondarily Aquatic Vertebrates. *University of California Press, California*, 65–81.

Segall M, Cornette R, Fabre A-C, Godoy-Diana R, Herrel A (2016) Does aquatic foraging impact head shape evolution in snakes? *Proceedings of the Royal Society B* **283**, 1–7.

Senn DG (1966) Uber das optische System im Gehirn squamater Reptilien. Eine vergleichend-morphologische Untersuchung, unter besonderer Berücksichtigung einiger Wühlschlangen. *Acta Anatomica. Supplementum* **52**, 1–87.

Senn DG, Northcutt RG (1973) The Forebrain and Midbrain of Some Squamates and Their Bearing on the Origin of Snakes. *Journal of Morphology* **140**, 135–152.

Shichida Y, Yamashita T, Imai H, Kishida T (2013) Evolution and Senses: Opsins, Bitter Taste, and Olfaction. Berlin, Germany: Springer, 46pp.

Shivik JA, Wright WG, Clark L (2000) Seasonal variability in brown tree snake (*Boiga irregularis*) response to lures. *Canadian Journal of Zoology* **78**, 79–84.

Smeets WJA, Hoogland PV, Lohman AH (1986) A Forebrain Atlas of the Lizard Gekko gecko. *The journal of Comparative Neurology* **254**, 1–19.

Smith NA, Clarke JA (2012) Endocranial Anatomy of the Charadriiformes: Sensory System Variation and the Evolution of Wing-Propelled Diving. *PLoSONE* **7**, e49584.

Souza NM, Maggs DJ, Park SA et al. (2015) Gross, histologic, and micro-computed tomographic anatomy of the lacrimal system of snakes. *Veterinary Ophthalmology* **18**, 15–22.

Starck D (1979) Cranio-Cerebral Relations in Recent Reptiles. In Gans, C., Northcutt, R.G., Ulinski, P. (eds) *Biology of the Reptilia (Neurology A),* Academic Press, London, New York and San Francisco, 462 pp.

Walsh SA, Barrett PM, Milner AC, Manley G, Witmer LM (2009) Inner ear anatomy is a proxy for deducing auditory capability and behaviour in reptiles and birds. *Proceedings of the Royal Society B: Biological Sciences* **276**, 1355–1360.

Walsh SA, Knoll MA (2011) Directions in Palaeoneurology. *The Palaeontological Association* **86**, 263–279.

Walsh SA, Milner A (2011) Evolution of the Avian Brain and Senses. In G. Dyke and G. Kaiser (eds) *Living Dinosaurs: The Evolutionary History of Modern Birds*, First Edition. Published by John Wiley & Sons, 282–305.

Willis KL, Christensen-Dalsgaard J, Ketten DR, Carr CE (2013) Middle Ear Cavity Morphology Is Consistent with an Aquatic Origin for Testudines. *PLoS ONE* **8**, e54086.

Witmer LM, Ridgely RC, Dufeau DL, Semones MC (2008) Using CT to Peer into the Past: 3D Visualization of the Brain and Ear Regions of Birds, Crocodiles, and Nonavian Dinosaurs. In:

Frey R, Endo H, editors. Anatomical Imaging: Towards a New Morphology. Tokyo. Springer-Verlag, 67–87.

Wyneken J (2007) Reptilian Neurology: Anatomy and Function. *Veterinary Clinics of North America: Exotic Animal Practice* **10**, 837–853.

Yi H, Norell MA (2015) The burrowing origin of modern snakes. *Science Advances* **1**, e1500743.

Zelditch ML, Swiderski DL, Sheets HD, Fink WL (2004) Geometric morphometrics for biologists: a primer. Academic Press, 443pp.

Supporting information

Appendix S1. Table of measurements taken on snake endocasts

Appendix S2. Table of measurements taken on the three *Python regius* specimens

Appendix S3. List of characters and matrix used for the PCoA

Appendix S4. Distribution of the variables in the principal component analyses performed on the 45 snake specimens.

1035 # Tables

1036 **Table 1.** List of the material analyzed. Ha represents the categories based on habitat: A,

1037 arboreal; F, fossorial; M, marine; T, terrestrial; SA, semi-aquatic. AH, Anthony Herrel

1038 personal collections; GD, Gheylen Daghfous personal collections.

1039

Family	Taxon	Ab.	Ha	Collection reference	Voxel size
Boidae	*Rhinotyphlops schlegelii*	Rs	F	AH Unnumb	13.3
Anomalepididae	*Typhlophis squamosus*	Ts	F	MNHN 1997.2042	5.1
Uropeltidae	*Uropeltis pulneyensis*	Up	F	MNHN 1994.0753	5.0
Cylindrophiidae	*Cylindrophis ruffus*	Cy	F	MNHN 1998.0201	20.1
Aniliidae	*Anilius scytale*	An	F	MNHN 1997.2106	10.1
Pythonidae	*Python regius*	P3	T	AH Unnumb	33.3
	Python regius	P2	T	AH Unnumb	28.9
	Python regius	P1	T	AH MS 37	21.6
Boidae	*Boa constrictor*	Bc	A	MNHN 1989.0177	7.6
	Candoia sp.	Cd	T	AH Unnumb	33.3
	Corallus hortulanus	Ch	A	AH MS 62	32
	Eunectes murinus	Em	SA	MNHN 1996.7898	7.6
Acrochordidae	*Acrochordus granulatus*	Ag	SA	ZRC 2.2334	24.2
Pareatidae	*Pareas margaritophorus*	Pm	A	MNHN 1974.1469	7.5
Viperidae	*Crotalus atrox*	Cr	T	AH MS 31	28.5
	Agkistrodon contortrix	Ac	T	AH MS 56	23.4
Homalopsidae	*Enhydris enhydris*	Ee	SA	ZRC 2.5507b	24.2
	Enhydris punctata	Ep	SA	ZRC 2.3554	24.2
	Cerberus rynchops	Ce	SA	MNHN-RA-1998.8583	35.3
	Homalopsis buccata	Hb	SA	ZRC 2.6411	24.2
	Erpeton tentaculatum	Et	SA	GD pers. coll.	7.5
	Bitia hydroides	Bh	M	ZRC 2.4374	20.9
	Fordonia leucobalia	Fl	SA	MNHN-RA-1912.26	33.2
	Cantoria violacea	Cv	SA	ZRC 2.3672	20.8
Lamprophiidae	*Mimophis mahfalensis*	Mm	T	MRSN R3171	24.7
	Atractaspis irregularis	Ai	F	MNHN 1999.9129	7.6
Elapidae	*Micrurus lemniscatus*	Ml	T	MNHN 1997.2353	7.6
	Naja nivea	Nn	T	AH MS 68	28.5
	Hydrophis elegans	He	M	MNHN-RA-0.1879	30.7
	Enhydrina schistosa	Es	M	ZRC 2.2043	20.8
	Astrotia stokesii	As	M	ZRC 2.2032	20.8

	Hydrophis major	Hm	M	MNHN 1990 4557	44.8
	Hydrophis ornatus	Ho	M	MNHN-RA-1994.6997	36
	Pelamis platurus	Pp	M	AH MS 64	31.9
	Aipysurus duboisii	Ad	M	MNHN-RA-1990.4519	41
	Aipysurus eydouxii	Ae	M	MNHN-RA-0.7704	40.2
	Microcephalophis gracilis	Mg	M	ZRC 2.2155	20.8
Natricidae	*Thamnophis sirtalis*	Ta	T	GD pers. coll.	7.5
Colubridae	*Chrysopelea ornata*	Co	A	MCZ R-177291	14.9
	Hierophis gemonensis	Hg	T	AH Unnumb	23.4
	Hierophis viridiflavus	Hv	T	AH Unnumb	19.2
	Dispholidus typus	Dt	A	AH Unnumb	32
	Boiga dendrophila	Bd	A	AH MS 102	18.2
	Dasypeltis sp.	Ds	A	MCZ 71877	14.9
	Coronella austriaca	Ca	T	AH MS 51	21.6

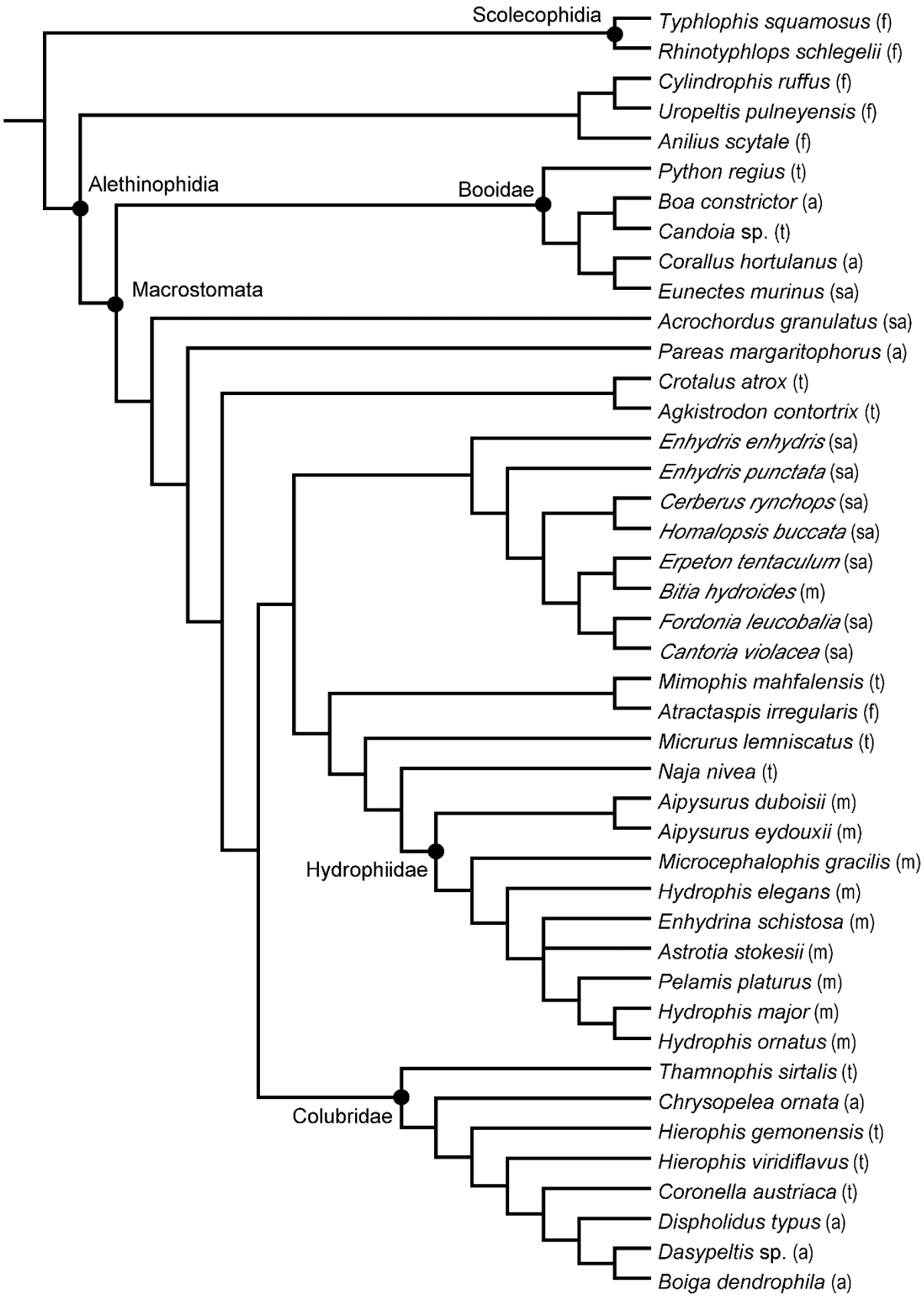
Scolecophidia
Typhlophis squamosus (f)
Rhinotyphlops schlegelii (f)
Cylindrophis ruffus (f)
Uropeltis pulneyensis (f)
Anilius scytale (f)
Alethinophidia
Booidae
Python regius (t)
Boa constrictor (a)
Candoia sp. (t)
Corallus hortulanus (a)
Eunectes murinus (sa)
Macrostomata
Acrochordus granulatus (sa)
Pareas margaritophorus (a)
Crotalus atrox (t)
Agkistrodon contortrix (t)
Enhydris enhydris (sa)
Enhydris punctata (sa)
Cerberus rynchops (sa)
Homalopsis buccata (sa)
Erpeton tentaculum (sa)
Bitia hydroides (m)
Fordonia leucobalia (sa)
Cantoria violacea (sa)
Mimophis mahfalensis (t)
Atractaspis irregularis (f)
Micrurus lemniscatus (t)
Naja nivea (t)
Aipysurus duboisii (m)
Aipysurus eydouxii (m)
Hydrophiidae
Microcephalophis gracilis (m)
Hydrophis elegans (m)
Enhydrina schistosa (m)
Astrotia stokesii (m)
Pelamis platurus (m)
Hydrophis major (m)
Hydrophis ornatus (m)
Thamnophis sirtalis (t)
Chrysopelea ornata (a)
Colubridae
Hierophis gemonensis (t)
Hierophis viridiflavus (t)
Coronella austriaca (t)
Dispholidus typus (a)
Dasypeltis sp. (a)
Boiga dendrophila (a)

1057

1058 **Fig. 1**. Schematic phylogenetic relationships of snakes sampled in the study (modified from
1059 Pyron et al., 2011; Hsiang et al., 2015; Lee and Scanlon, 2002). Principal ecology/habitat:
1060 fossorial (f), terrestrial (t), arboreal (a), semi-aquatic (sa), marine (m).
1061

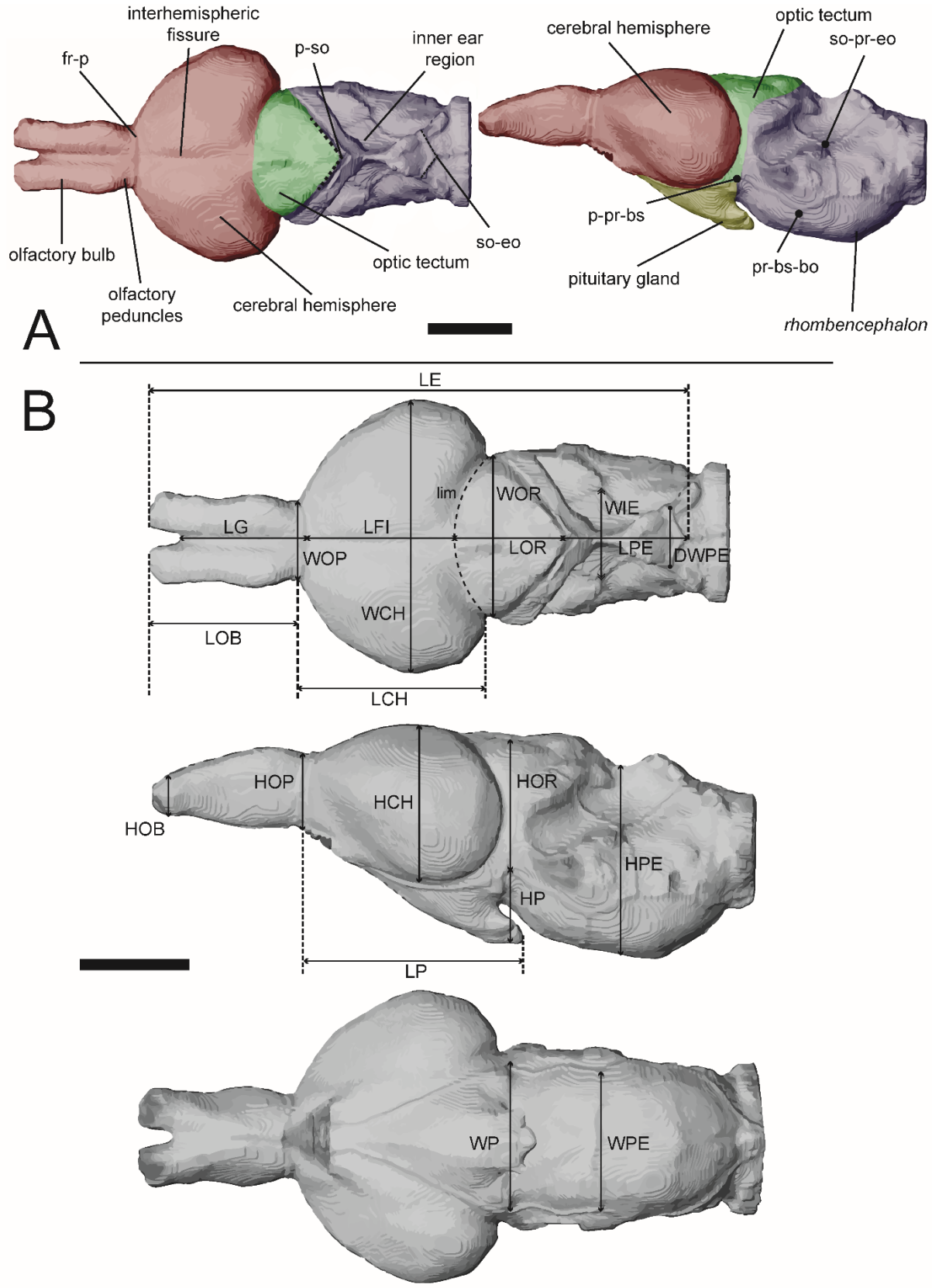
A
interhemispheric fissure
fr-p
p-so
inner ear region
olfactory bulb
olfactory peduncles
optic tectum
so-eo
cerebral hemisphere
cerebral hemisphere
optic tectum
so-pr-eo
p-pr-bs
pituitary gland
pr-bs-bo
rhombencephalon
B
LE
lim
WOR
WIE
LG
LFI
LOR
LPE
DWPE
WOP
WCH
LOB
LCH
HOP
HCH
HOR
HOB
HPE
HP
LP
WP
WPE

1062

1063

Fig. 2. Reconstructed brain endocast of *Enhydris punctata* (Homalopsidae) **(A)**, Illustration of the major structures seen in dorsal and left lateral views: telencephalon (red), diencephalon (yellow), mesencephalon (green), rhombencephalon (purple); **(B)**, Illustration of the various measurements defined in Material and Method and taken in dorsal, left lateral and ventral views. **Abbreviations: fr-p**, fronto-parietal suture; **lim**, groove between the optic tectum and the cerebral hemispheres; **p-pr-bs**, triple point formed by the sutures between the parietal, prootic and basisphenoid; **p-so**, parietal-supraoccipital suture; **pr-bs-bo**, triple point formed by the suture between the prootic, basisphenoid and basioccipital; **so-eo**, supraoccipital-exoccipital suture; **so-pr-eo**, triple point formed by the sutures of the supraoccipital, prootic and exoocipital; **DWPE**, Dorsal width of the posterior end of the brain endocast; **HCH**, Maximal height of the cerebral hemisphere; **HOB**, Height of the main olfactory bulb; **HOP**, Height of the olfactory peduncle; **HOR**, Height of the optic tectum; **HP**, Height of the pituitary bulb; **HPE**, Height of the posterior part of the brain endocast; **LCH**, Lateral expansion of the cerebral hemispheres; **LE**, Length of the brain endocast; **LFI**, Length of the interhemispheric fissure; **LG**, Length of the groove between olfactory bulbs; **LOB**, Length of the olfactory bulbs; **LOR**, Length of the optic tectum; **LP**, Length of the pituitary bulb; **LPE**, Length of the posterior part of the brain endocast; **WCH**, Maximal width of the cerebral hemispheres; **WIE**, Width in the inner ear region; **WOP**, Width of the olfactory peduncles; **WOR**, Maximal width of the optic tectum; **WP**, Width in the pituitary gland region; **WPE**, Width of the ventral part of the brain endocast. Scale bar equals to 2 mm.

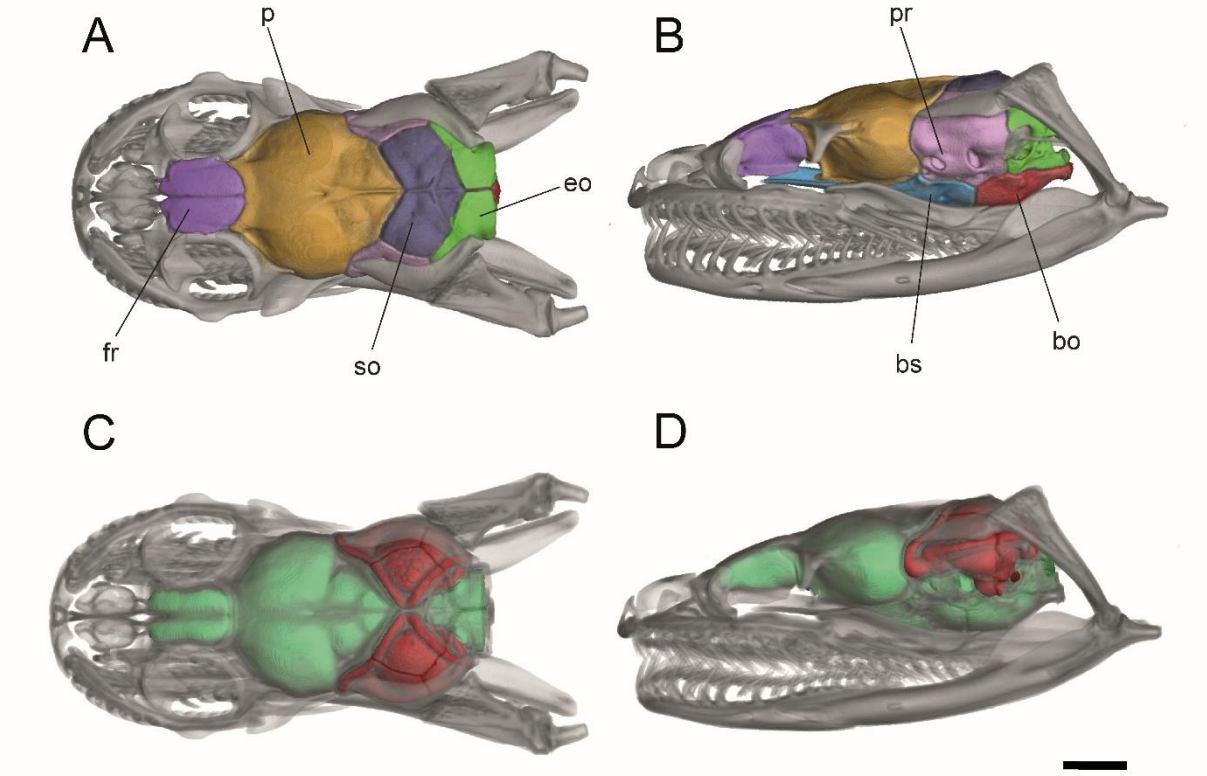

1085

1086 **Fig. 3.** Skull of *Enhydris punctata* (Homalopsidae) in dorsal (A) and left lateral (B) views

1087 showing the bones surrounding the brain endocast; (C-D) with bones rendered transparent to

1088 reveal the brain endocast (green) and the inner ear (red). **Abbreviations: bo**, basioccipital; **bs**,

1089 basisphenoid; **eo**, exoccipitals; **fr**, frontal; **p**, parietal; **pr**, prootics; **so**, supraoccipitals. Scale

1090 bar equals 2 mm.

1091

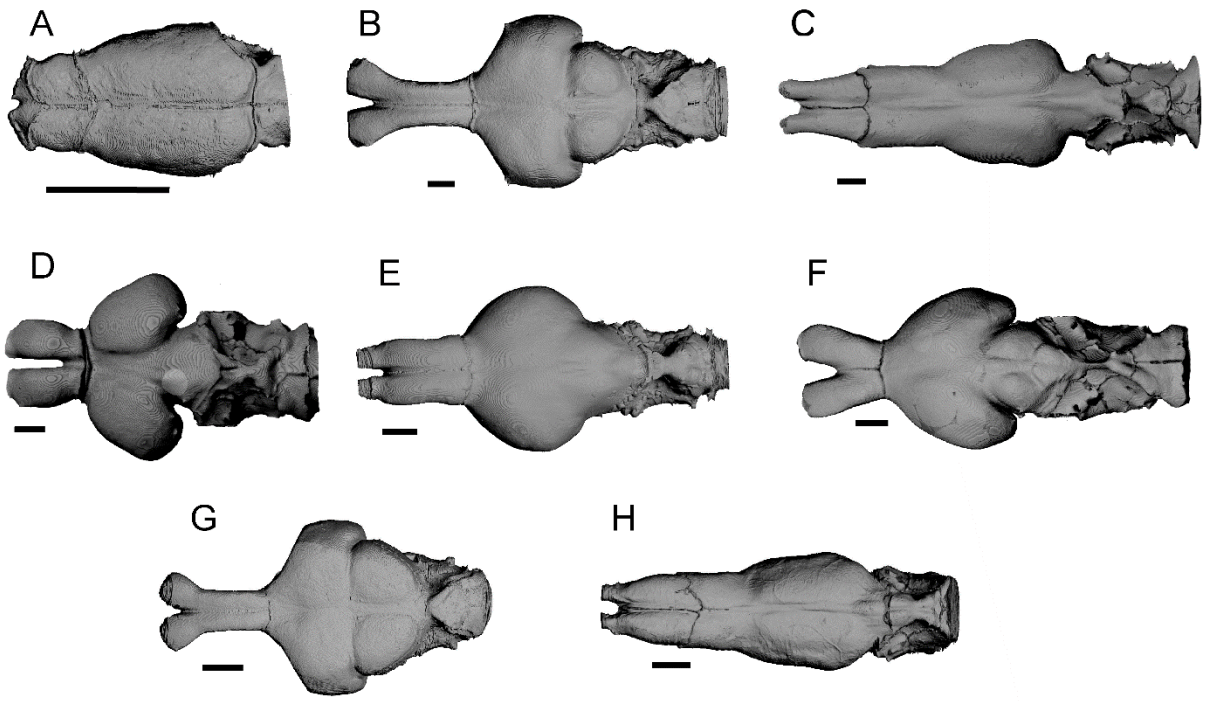

Fig. 4. Brain endocasts in dorsal view of **(A)** *Typhlophys squamosus* (Typhlopidae); **(B)** *Hierophis viridiflavus* (Colubridae); **(C)** *Cylindrophis ruffus* (Cylindrophiidae); **(D)** *Acrochordus granulatus* (Acrochordidae); **(E)** *Eunectes murinus* (Boidae); **(F)** *Homalopsis buccata* (Homalopsidae); **(G)** *Chrysopelea ornata* (Colubridae); **(H)** *Anilius scytale* (Aniliidae). Scale bars equal 1mm.

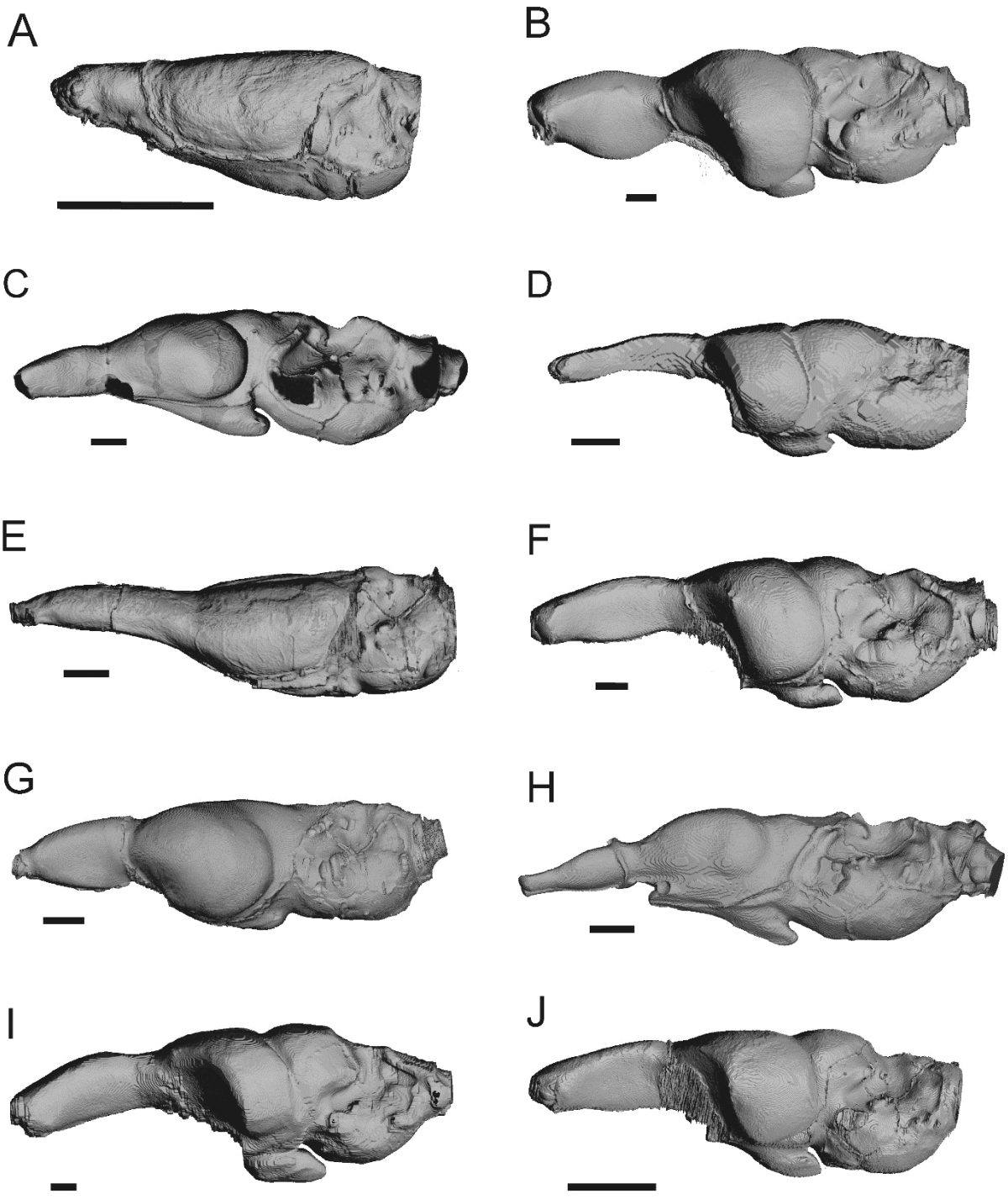

Fig. 5. Brain endocasts in left lateral view of **(A)** *Typhlophys squamosus* (Typhlopidae); **(B)** *Boiga dendrophila* (Colubridae); **(C)** *Homalopsis buccata* (Homalopsidae); **(D)** *Mimophis mahfalensis* (Lamprophiidae); **(E)** *Anilius scytale* (Aniliidae); **(F)** *Hierophis viridiflavus* (Colubridae); **(G)** *Eunectes murinus* (Boidae); **(H)** *Enhydrina schistosa* (Elapidae); **(I)** *Dispholidus typus* (Colubridae); **(J)** *Thamnophis sirtalis* (Natricidae). Scale bars equal 1mm.

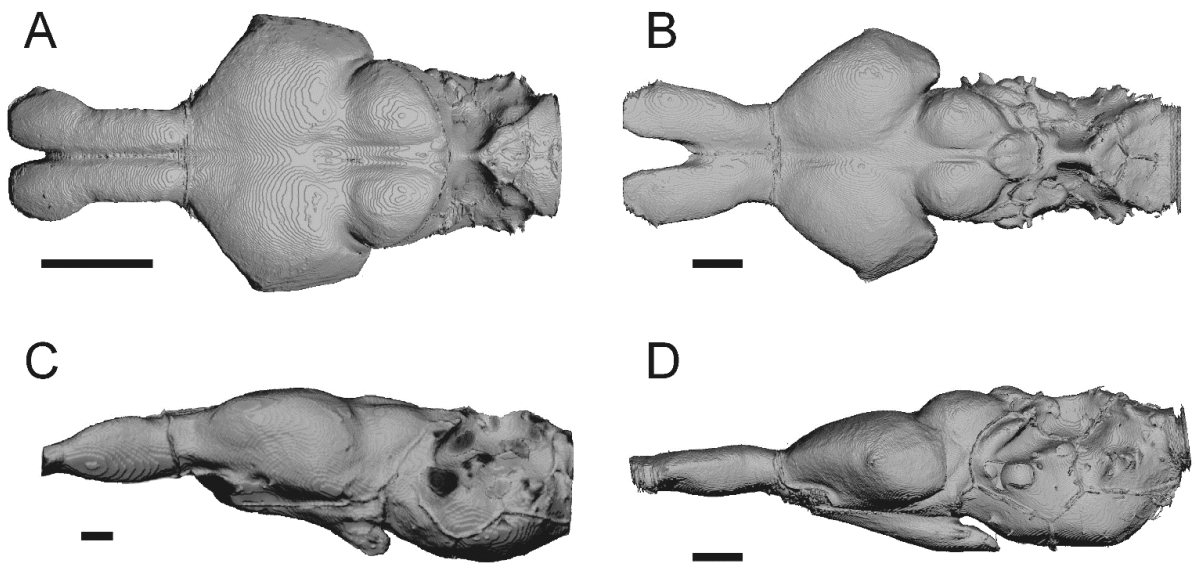

Fig. 6. Brain endocasts in dorsal (upper row) and left lateral (lower row) views of **(A)** *Thamnophis sirtalis* (Natricidae); **(B)** *Erpeton tentaculatum* (Homalopsidae); **(C)** *Hydrophis major* (Elapidae); **(D)** *Erpeton tentaculatum*. Scale bars equal 1mm.

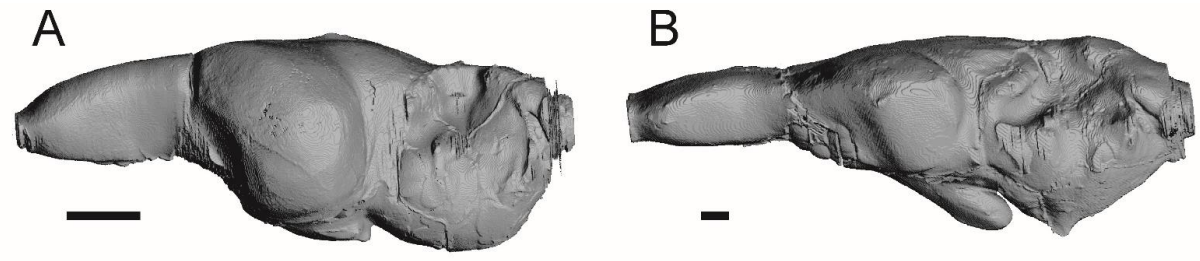

Fig. 7. Brain endocasts in left lateral view of **(A)** *Boa constrictor* (Boidae); **(B)** *Crotalus atrox* (Viperidae). Scale bars equal 1mm.

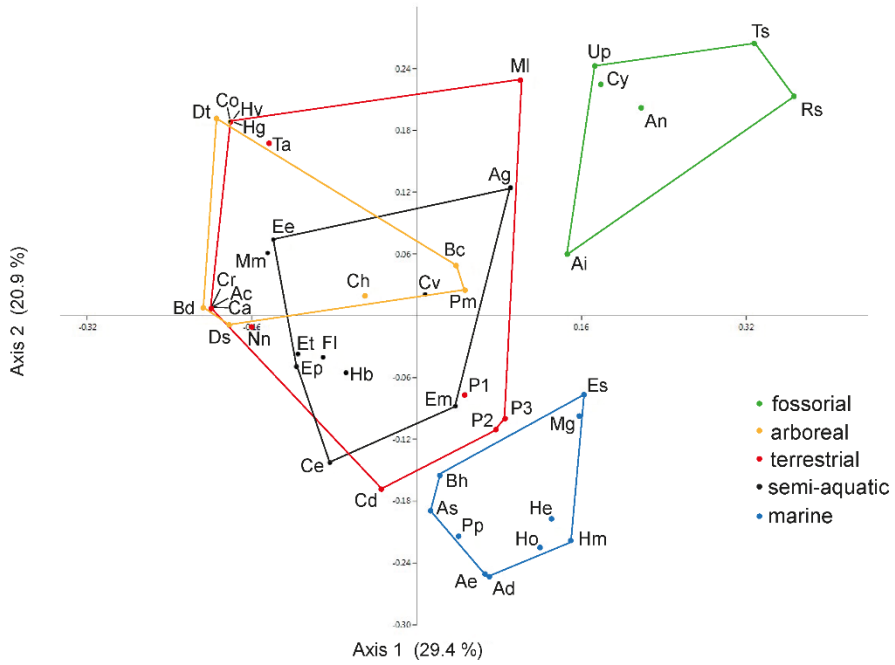

1115

1116 **Fig. 8.** Results of the principal coordinate analysis performed on the snake brain endocast

1117 characters (Supplementary Data S3). See Table 1 for name abbreviations.

1118

1119

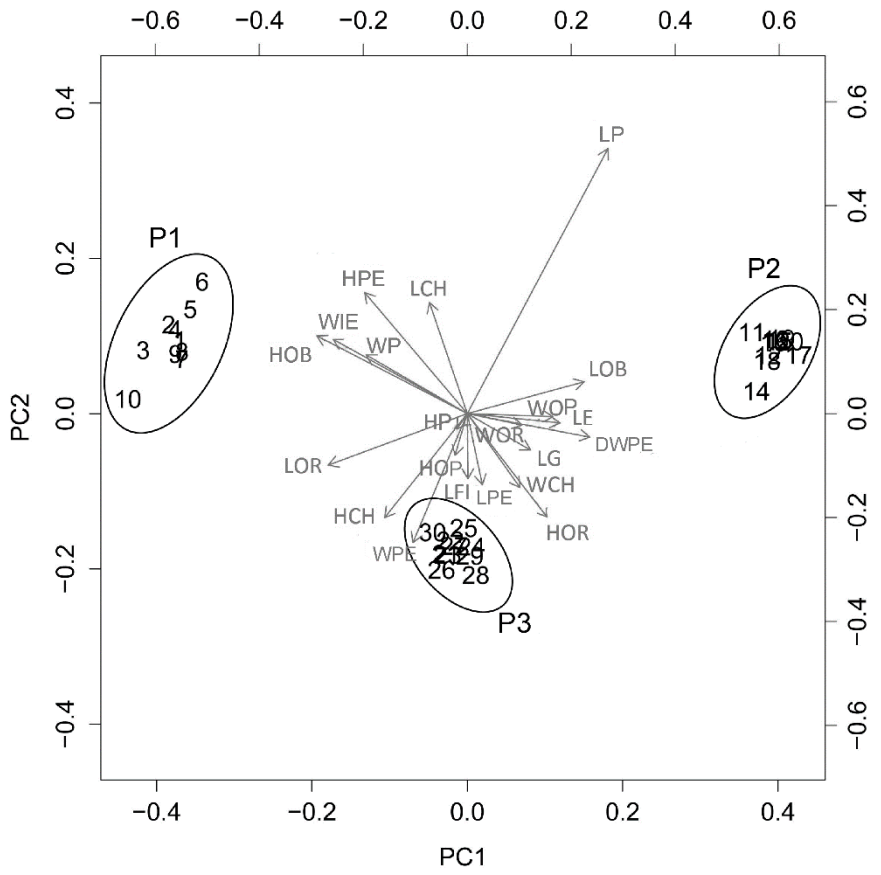

Fig. 9. Results of the principal component analysis performed on the brain endocast variables for three *Python regius* specimens, (P1) smaller specimen, (P3) intermediate specimen, (P2) largest specimen. Scatter plot illustrating the position of the different specimens on the first two principal components. **Abbreviations: DWPE**, Dorsal width of the posterior end of the brain endocast; **HCH**, Maximal height of the cerebral hemisphere; **HOB**, Height of the main olfactory bulb; **HOP**, Height of the olfactory peduncle; **HOR**, Height of the optic tectum; **HP**, Height of the pituitary bulb; **HPE**, Height of the posterior part of the brain endocast; **LCH**, Lateral expansion of the cerebral hemispheres; **LE**, Length of the brain endocast; **LFI**, Length of the interhemispheric fissure; **LG**, Length of the groove between olfactory bulbs; **LOB**, Length of the olfactory bulbs; **LOR**, Length of the optic tectum; **LP**, Length of the pituitary gland; **LPE**, Length of the posterior part of the brain endocast; **WCH**, Maximal width of the cerebral hemispheres; **WIE**, Width in the inner ear region; **WOP**, Width of the olfactory

peduncles; **WOR**, Maximal width of the optic tectum; **WP**, Width in the pituitary gland region; **WPE**, Width of the ventral part of the brain endocast.

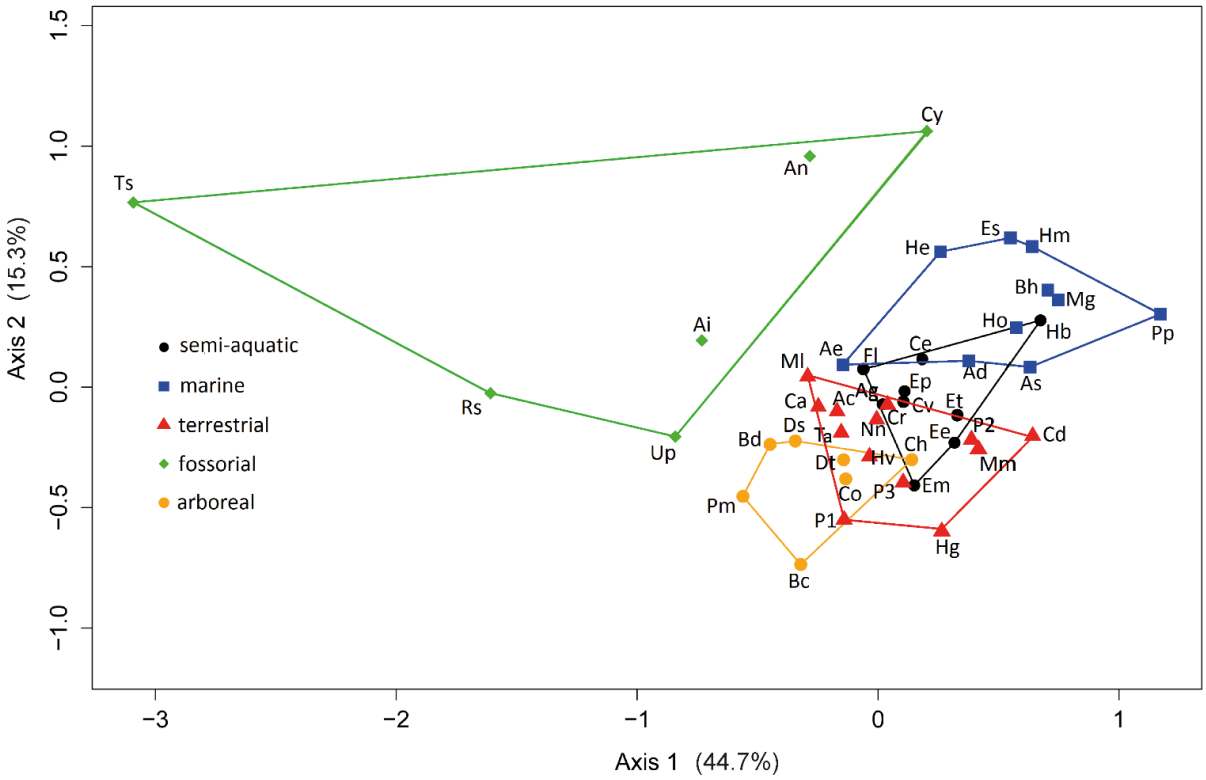

Fig. 10. Results of the principal component analyses performed on the snake brain endocast variables of the 45 specimens. Scatter plot illustrating the position of the different species on the first and second principal components and figuring the different ecologies. See Table 1 for name abbreviations.

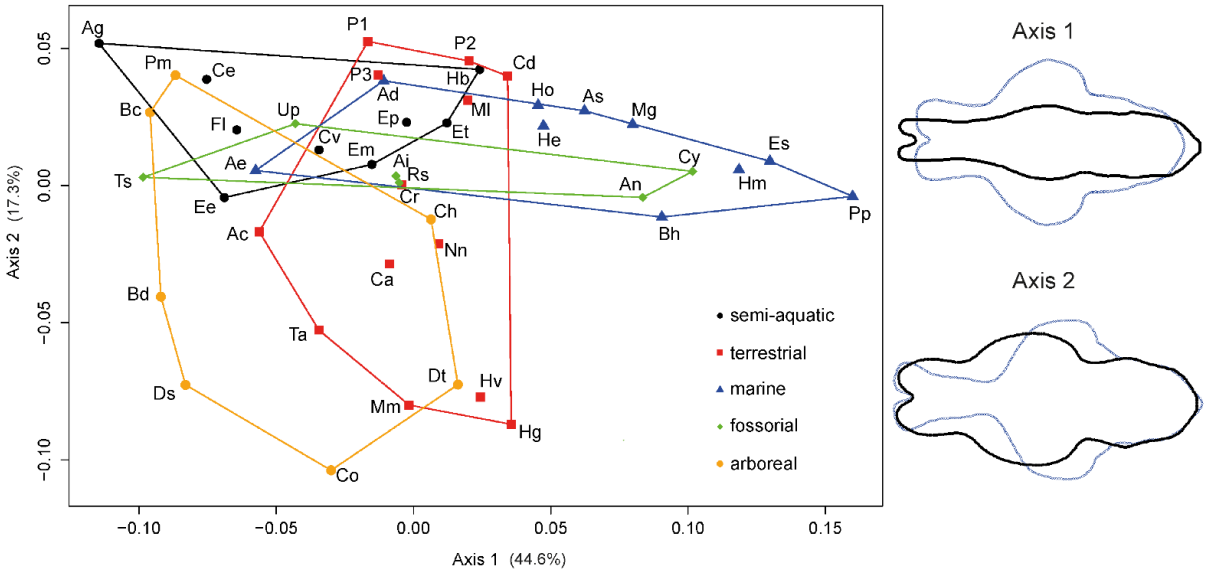

Fig. 11. Results of the principal component analyses performed on the snake brain endocast outline curves in ventral view. The blue and dark dotted lines indicate respectively the low and high values along the two axes. See Table 1 for name abbreviations.

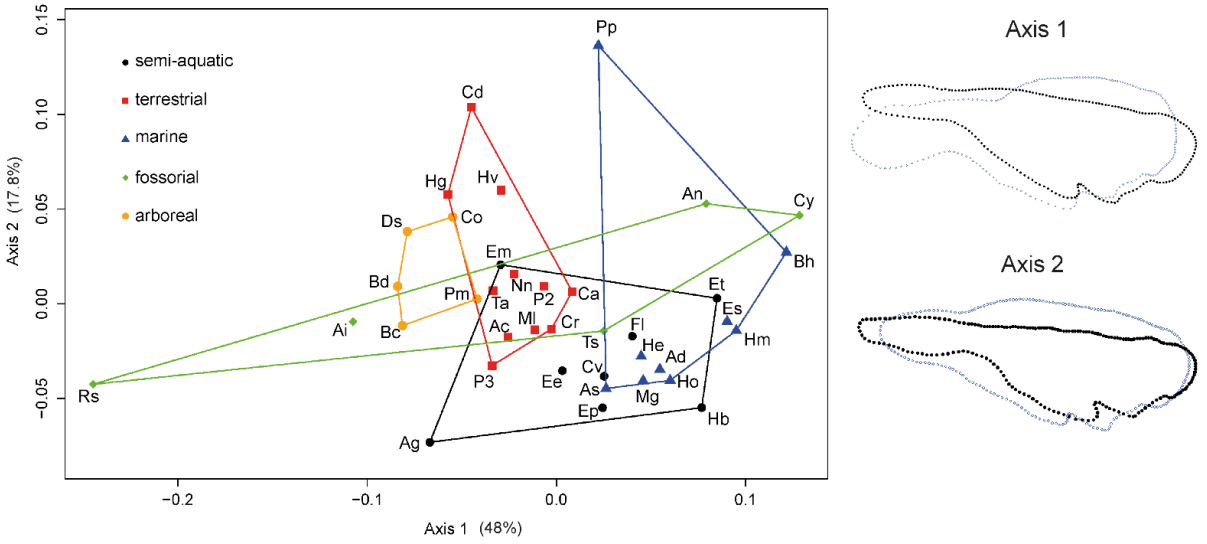

Fig. 12. Results of the principal component analyses performed on the snake brain endocast outline curves in lateral view. The blue and dark dotted lines indicate respectively the low and high values along the two axes. See Table 1 for name abbreviations.